AD-A090 475 CALIFORNIA UNIV LOS ANGELES DEPT OF MATERIALS SCIEN--ETC F/G 20/1
CONTRIBUTIONS TO THE ACOUSTIC EMISSION SYMPOSIUM (5TH), TOKYO, --ETC(U)
OCT 80 K ONO, S - HSU, K OKAJIMA, M YAMAMOTO N00014-75-C-0419
UNCLASSIFIED TR-80-03 NL

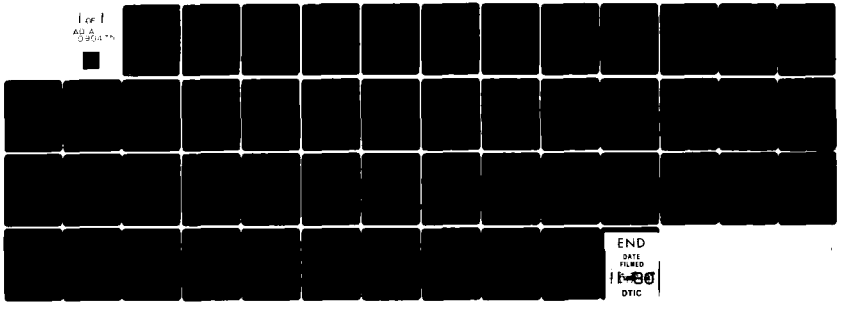

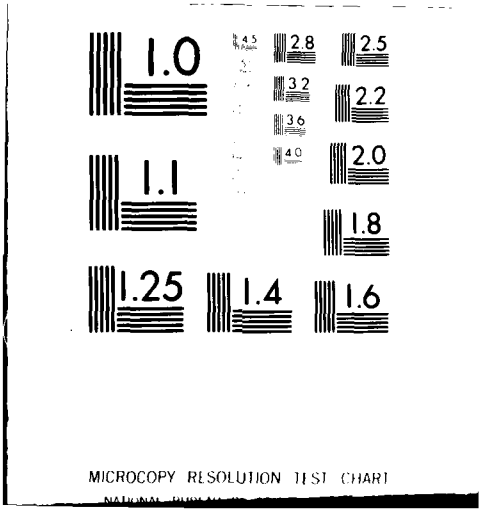
1.0
1.1
1.25
1.4
1.6
1.8
2.0
2.2
2.5
2.8
3.2
3.6
4.0
4.5
MICROCOPY RESOLUTION TEST CHART

Technical Report No. 80-03

to the

Office of Naval Research

Contract No. N00014-75-C-0419

CONTRIBUTIONS TO THE FIFTH ACOUSTIC EMISSION SYMPOSIUM

K. Ono, S.-Y.S. Hsu, K. Okajima,
M. Yamamoto and C. Ouchi

Materials Science and Engineering Department
School of Engineering and Applied Science
University of California
Los Angeles, California 90024

October 1980

(14) TR-80-03

SECURITY CLASSIFICATION OF THIS PAGE (When Data Entered)

REPORT DOCUMENTATION PAGE

READ INSTRUCTIONS BEFORE COMPLETING FORM

1 REPORT NUMBER: ONR Technical Report No. 80-03

2. GOVT ACCESSION NO.: AD-A090475

3. RECIPIENT'S CATALOG NUMBER:

(6) 4. TITLE (and Subtitle): Contributions to the Fifth Acoustic Emission Symposium (5th, Tokyo), 18-21 Nov. 1980

(9) 5. TYPE OF REPORT & PERIOD COVERED: Technical rept.

6. PERFORMING ORG. REPORT NUMBER:

(10) 7. AUTHOR(s): Kanji Ono, S.-Y.S. Hsu, K. Okajima, M. Yamamoto and C. Ouchi

(15) 8. CONTRACT OR GRANT NUMBER(s): N00014-75-C-0419

9. PERFORMING ORGANIZATION NAME AND ADDRESS: Materials Science and Engineering Department, University of California, Los Angeles, CA 90024

10. PROGRAM ELEMENT, PROJECT, TASK AREA & WORK UNIT NUMBERS:

11. CONTROLLING OFFICE NAME AND ADDRESS: Physics Program, ONR-800 North Quincy Street, Arlington, Virginia 22217

(11) 12. REPORT DATE: October 1980

13. NUMBER OF PAGES: 48

14. MONITORING AGENCY NAME & ADDRESS (if different from Controlling Office):

(12) 54

15. SECURITY CLASS. (of this report): Unclassified

15a. DECLASSIFICATION DOWNGRADING SCHEDULE:

16. DISTRIBUTION STATEMENT (of this Report)

Unlimited

This document has been approved for public release and sale; its distribution is unlimited.

17. DISTRIBUTION STATEMENT (of the abstract entered in Block 20, if different from Report)

18 SUPPLEMENTARY NOTES

To be presented at the Fifth Acoustic Emission Symposium, 18-20 November 1980, Tokyo, Japan, and to be published in its Proceedings volume by the Japanese Society of Nondestructive Inspection.

19. KEY WORDS (Continue on reverse side if necessary and identify by block number)

Acoustic Emission
Iron, Steel, Nickel
Aluminum, Copper
Cu-Zn and Cu-Ni Alloys
Heat Treatment
Nonmetallic Inclusions
Deformation
Fracture Tests

20 ABSTRACT (Continue on reverse side if necessary and identify by block number)

This report consists of four papers to be given at the Fifth Acoustic Emission Symposium. For detailed contents, see the abstract of each paper.

DD FORM 1 JAN 73 1473 EDITION OF 1 NOV 65 IS OBSOLETE
S/N 0102 LF 014 6601

406237

SECURITY CLASSIFICATION OF THIS PAGE (When Data Entered)

ACOUSTIC EMISSION OF PLASTIC FLOW - I. METALS

S.-Y. S. Hsu and K. Ono
Materials Science and Engineering
School of Engineering and Applied Science
University of California
Los Angeles, California 90024 USA

ABSTRACT

This paper reports the first part of comprehensive study on AE of plastic flow. While a number of theoretical and experimental studies have been conducted, the understanding of dislcoation related AE has remained an elusive target. In our study, a theoretical model of continuous AE, previously proposed by Ono, has been developed further, including the operation of dislocation sources, unpinning, the distribution of internal stress and the drag term of dislocation motion. The model forms the basis of discussion on temperature, strain and strain rate dependencies of AE during tensile deformation of aluminum, copper and iron. Variations of dislocation substructures and the phonon drag term on moving dislocations will be introduced as important parameters controlling AE behavior in polycrystalline metals.

INTROUDUCTION

Acoustic emission (AE) from metals during plastic deformation has been investigated extensively over the last forty years. Results of these studies have been reviewed recently by Carpenter and Heiple[1] and Kishi and Kuribayashi.[2] It has been agreed that dislocation movement is the basic source of AE, but to date we have attained no concensus as to the mechanisms of AE.

In order to understand the AE behavior of materials undergoing plastic deformation, we have selected pure Aℓ and Cu, both fcc, and Fe. These materials were chosen because their mechanical properties, microstructures and deformation mechanisms have been subjected to extensive investigations, and well documented. The deformation mechanisms of these metals are simpler than those of alloys, because the obstacles resisting the dislocation motion are mainly other dislocations in fcc metals and the intrinsic lattice friction and dislocation substructures in iron.

In this study, temperature dependence of AE behavhior of Aℓ, Cu and Fe were studied in detail. With the increase of testing temperature, dislocation, behavior changes from the lattice friction controlled (bcc) and dislocation interaction dominated (bcc and fcc) ones at low temperatures to dynamic recovery or dynamic recrystallization at elevated temperatures. The AE results will be discussed in terms of the dislocation related AE theories, as well as microstructural features.

EXPERIMENTALS

The purities of the materials were 99.99% for Aℓ and Cu, and 99.4% for iron. Tensile specimen was in sheet form with overall size of 305mm x 25mm and the

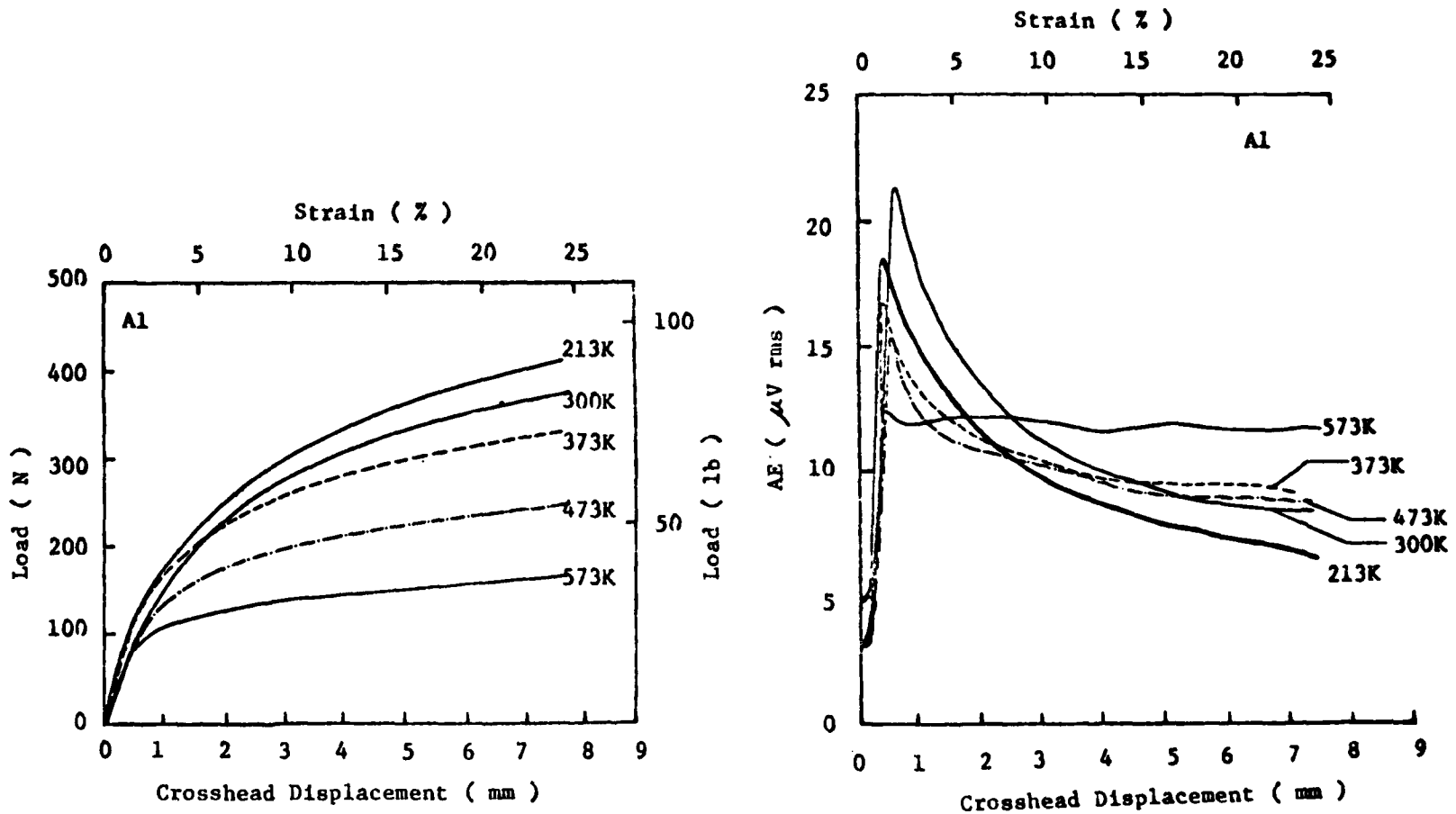

Fig. 1 Load-elongation and V_r-strain curves of aluminum at different temperatures.

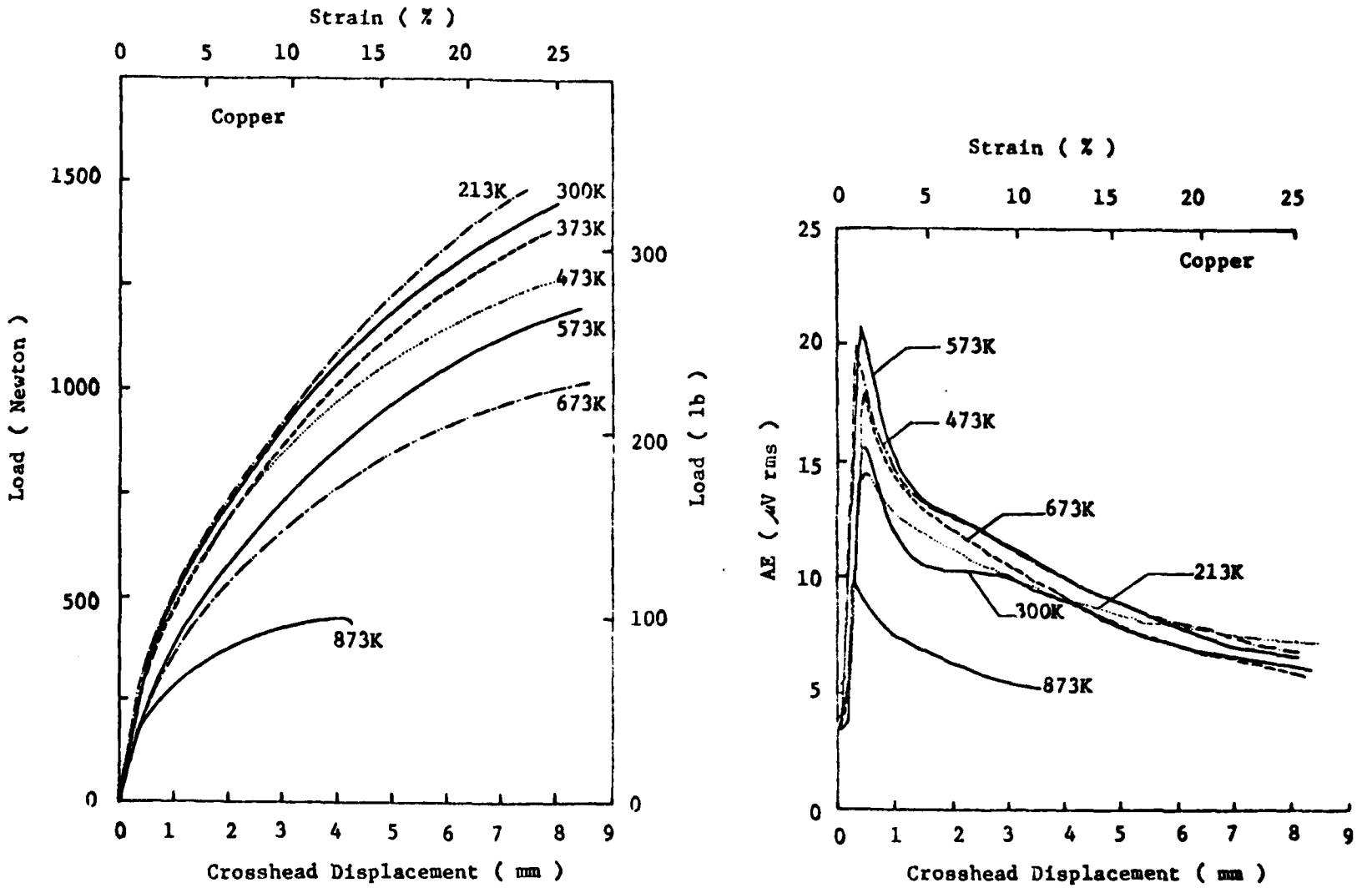

Fig. 2 Load-elongation and V_r-strain curves of copper at different temperatures.

thickness of 1.2mm (2.8mm for Fe). The reduced gage section was 32mm long and 6.4mm wide. For Aℓ and Cu, a stainless steel rod 9.5mm in diameter and 150mm long was used as a waveguide. One end of the rod was either glued or brazed to the specimen and a 100 kHz PZT-5A transducer element was coupled to the other end of the waveguide with beeswax. The transducer output was fed to a root mean square (r.m.s.) voltmeter through a 60 dB preamplifier with a 50 ~ 125 KHz bandpass filter. High temperature testing was conducted in air using a small nichrome wound furnace. For iron, the high temperature testing was performed in a vacuum furnace backfilled with helium. For this reason, a bent waveguide was welded to each iron specimen and the transducer was placed in a water-cooled section of the sealed furnace. Compared with the straight waveguide, the bent waveguide reduced AE output signals by 3 dB. The grips of the specimens were preloaded. The specimen was deformed under a constant crosshead speed of 1.27mm/min, which corresponded to a nominal strain rate of 7×10^{4}/s.

RESULTS

The load-strain curves and the AE responses of Aℓ tested at different temperatures are shown in Fig. 1. The yield strength is relatively insensitive to the deformation temperature, while the work-hardening rate declined steadily with increasing temperature. The AE behavior (V_r-strain curve) exhibited a fast increase of output signal levels during the pre-yielding region, and reached a maximum value near macroscopic yielding. The rate of decrease of AE output levels beyond yielding depended on the work-hardening rate. At 573°K, the work-hardening rate approached zero in the load-elongation curve and the AE output level remained relatively constant after the macroscopic yielding. The peak AE level at yielding was highest at 300°K, decreasing to 60% of the maximum value at 573°K. A lower deformation temperature also reduced the peak AE level at yielding.

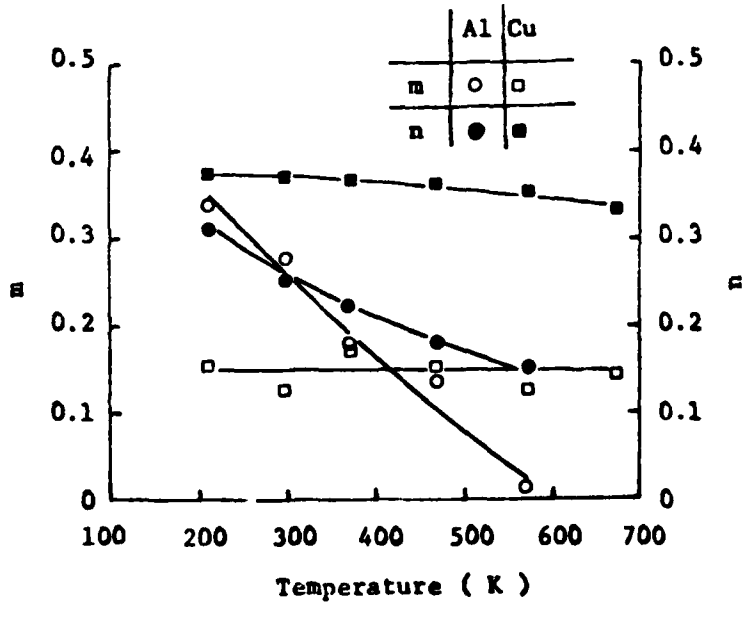

Fig. 3 Variations of m and n of Aℓ and Cu with testing temperatures.

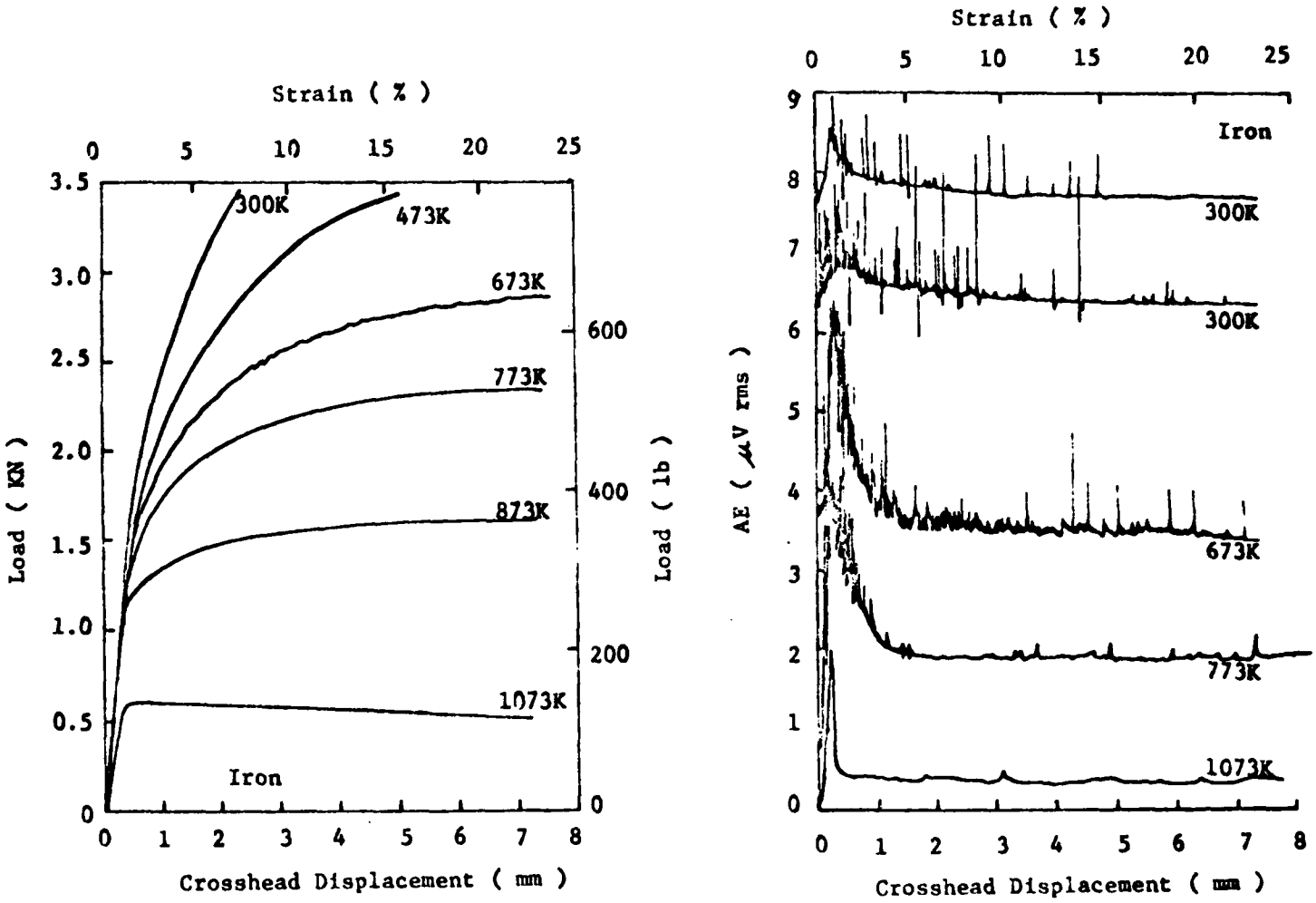

Fig. 4 Load-elongation and V_r-strain curves of iron at different temperatures.

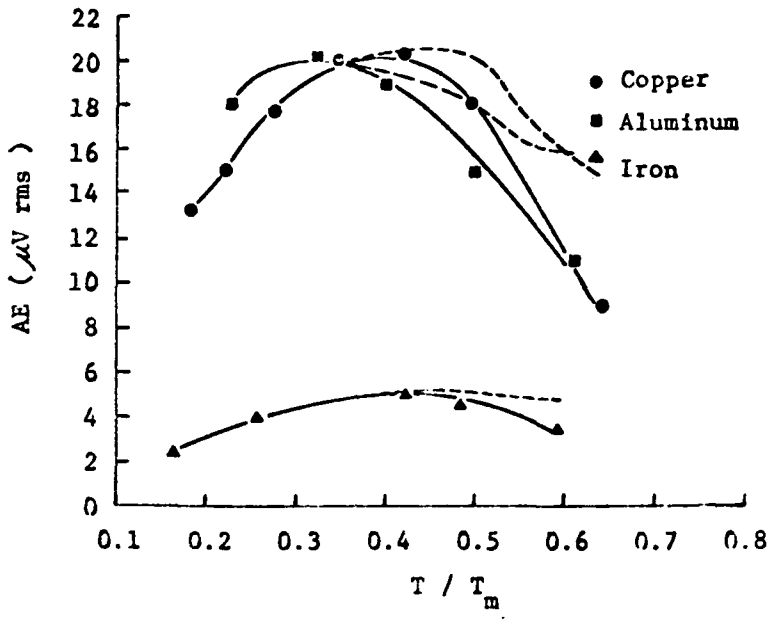

Fig. 5 Temperature dependence of peak AE output levels of Aℓ, Cu and Fe.

In Cu, the shape of V_r-strain curves was basically unchanged from 200 to 873°K. The AE level reached a peak at macroscopic yielding and declined upon further deformation. The peak AE level at yielding was maximum at 573°K, decreasing at higher and lower test temperatures. The stress-strain curves always showed typical parabolic behavior with decreasing work-hardening rates at higher temperatures. However, the observed decrease in the work-hardening rates was not as pronounced in Cu than in Aℓ. This is shown clearly in Fig. 3, where the exponent n of the power-law work hardening behavior is plotted against test temperature. Here n is defined by

$$\sigma = K \epsilon_p^{\,n} \quad , \tag{1}$$

where σ is stress, ϵ_p is plastic strain and K is a constant. In Cu, n remained above 0.3 up to 673°K, while n decreased from 0.3 to 0.15 between 200 and 573°K in Aℓ. The decreasing part of a V_r-strain curve can be expressed by

$$V_r(\epsilon_p) = C \epsilon_p^{\,-m} \tag{2}$$

where C and m are constants.[3] The values of m for Aℓ and Cu are also plotted in Fig. 3. While m for Cu remained nearly unchanged at 0.15, m for Aℓ decreased from 0.33 at 200°K to 0.01 at 573°K.

The load-strain curves of iron are shown in Fig. 4, along with the corresponding V_r-strain curves. No initial discontinuous yielding was observed at all temperatures, but at 673°K serrations appeared during work hardening. The V_r-strain curves contained many small burst signals, $3 \sim 4 \mu V$ in magnitude, especially within the initial few percent of plastic strain. Most of these spikes were probably due to spurious sources, because an iron specimen deformed at 300°K using a different experimental set-up contained much few spikes (the top V_r-strain curve at 300°K in Fig. 4). At 673°K small fluctuations in V_r-strain curve can be distinguished from background levels. The observed AE levels were generally low, even after the correction for the different waveguide arrangement. The peak AE level increased from about $2 \mu V$ at 300°K to $5 \mu V$ at 773°K, but it decreased to about $3 \mu V$ at 1073°K. The V_r-strain curves for Fe could not be fitted to Eq. (2) by a single m value, atlthough m for small strains remained nearly constant from 300 to 773°K.

The peak AE output levels near macroscopic yielding for Aℓ, Cu and Fe are plotted in Fig. 5 as the function of homologous temperature. The dash lines represents the corrected peak AE output levels, taking into account of the wave attenuation effect at high temperatures. All three materials showed a maximum in the peak AE output levels at temperature T_c of 0.3 to 0.4 T_m (T_m is the absolute melting temperature of the material). Between 0.2 and 0.6 T_m, A and Cu had similar AE output levels, ranging from $15 \mu V$ to $22 \mu V$ after correction. On the other hand, Fe was a quite material throughout the entire temperature range tested, and the corrected peak AE level saturated above 0.4 T_m.

DISCUSSION

Following Malen and Bolin,[4] Ono[5] recently derived the transducer response to an instantaneous increment of inelastic strain as

$$R_m = C \, \Delta\epsilon^* / \tau, \tag{3}$$

where R_m is the peak voltage of the transducer response, $\Delta\epsilon^*$ is a strain increment, 4τ is the rise time increasing from 0.1 to $0.9 \Delta\epsilon^*$ and C is a constant. During plastic deformation, $\Delta\epsilon^*$ represents the plastic strain of a slip step, which typically consists of more than one dislocation segment sweeping between obstacles. Thus, we have for a constant strain-rate tensile test

$$\dot{N} = \dot{\epsilon} / \Delta\epsilon^*, \tag{4}$$

where $\dot{N}$ is the number of slip steps per unit time. For continuous signals comprised of a large number of slip steps exciting a transducer at random, the rms voltage output from the transducer V_r is given by

$$V_r = C' \sqrt{\dot{N}} \, \Delta\epsilon^* / \tau \, , \tag{5}$$

where $\dot{N}$ is the average number of excitation. Hsu[6] has further refined the theoretical model, decomposing the time dependence of a strain increment into the unpinning and operation of a dislocation source, free flight of a dislocation segment under the influence of internal stress and viscous phonon drag and the deceleration at an obstacle. When the Hsu model is applied to a typical work-hardening material with forest dislocations as the primary obstacles, Eq. (5) can be rewritten as

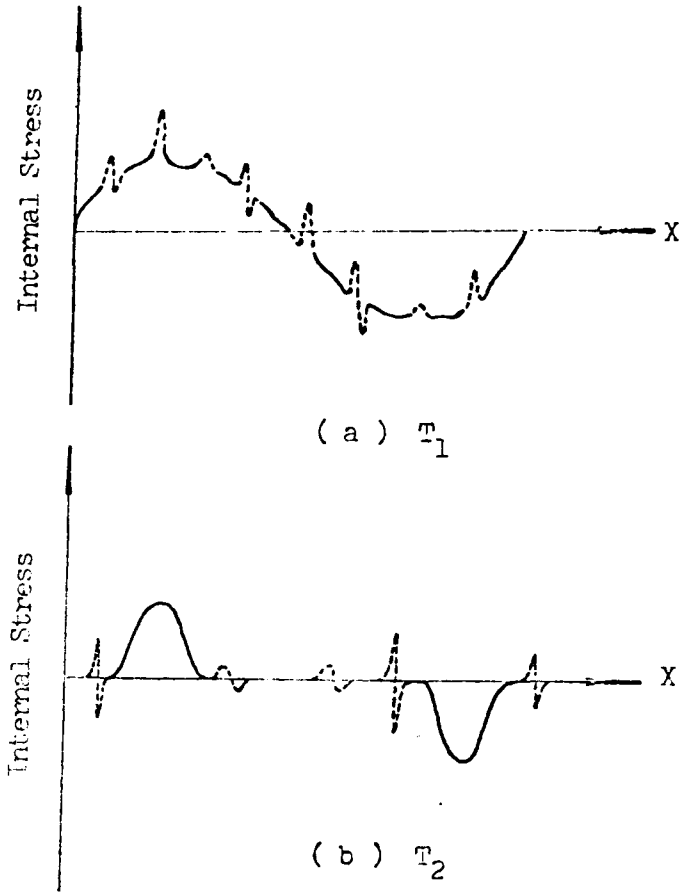

Fig. 6 Effects of temperatures on the internal stress field encountered by a dislocation moving through the slip-plane. $T_2 > T_1$.

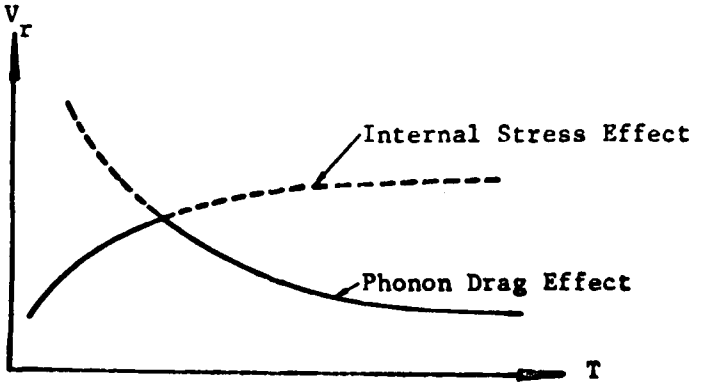

Fig. 7 Combined effect of internal stress and phonon drag on the peak AE output at different temperatures.

$$V_r = C'' \bar{v} \sqrt{N_m \cdot \ell} \qquad (6)$$

where C" is a constant, $\bar{v}$ is the average free flight velocity of moving dislocations, N_m is the density of mobile dislocations and ℓ is the average length of dislocation segments, respectively. The predicted dependence on N_m and ℓ in Eq. (6) is identical to that derived by Kiesewetter and Schillar[7] on the basis of the energy dissipation of moving dislocations. However, the $\bar{v}$ term accounts for the activation of dislocation sources and the viscous drag effect.

A typical AE behavior of pure metals can be understood by combining the present AE source model and the established dislocation behavior of these materials. As the applied stress is raised, dislocation sources, often at grain boundaries, start to operate; that is, N_m increases. At this stage, ℓ and $\bar{v}$ are controlled by grain size, and remain relatively unchanged. Consequently, the AE level as well as plastic strain rate, increase with increasing stress.[1] As the macroscopic yield stress is reached, the number of dislocations becomes substantially higher and the dislocation interaction supplants as the controlling factor for ℓ and $\bar{v}$. The total dislocation density typically increase linearly with strain, decreasing ℓ inversely proportional to strain. Effects of work hardening on N_m and v are complex, but are generally expected to reduce them at higher strain. The relationship between N_m or $\bar{v}$ and strain cannot be determined experimentally at present. A few theoretical models have been proposed, one of which will be referred to in a later discussion.

Dislocation velocity measurements have shown that v is linear with stress in Cu and Aℓ,[8] whereas v increases with $\sigma^{2 \sim 3}$ in Fe.[9] Stronger stress dependence in Fe is believed to be due to the lattice friction, especially on screw dislocations. Thus, v in Fe is expected to be less than in fcc metals, which also leads to lower V_r according to Eq. (6).

The free-flight velocity of the mobile dislocation is affected by drag coefficient B and the distribution of the internal stress field, given by

$$\bar{v} = \lambda / \int_0^{\lambda} \frac{B\,dx}{b[\sigma_a - \sigma_i(x)]} \qquad (5)$$

where λ is the mean free path of dislocations, B is the dislocation drag coefficient, b is the Burgers vector, σ is the applied stress and $\sigma_i(x)$ is the internal stress field, respectively. When the deformation temperature increases, the electron microscope observations reveal the changes in the arrangements of dislocations in Aℓ, Cu and Fe. At low deformation temperatures, dislocations are more uniformly distributed, but, as T_D increases, the dislocation cell walls become more well defined, and the cell interior regions become dislocation free.[13-17] These observations suggest that the internal stress distribution changes from short period at low T_D to long period at higher T_D, as indicated in Fig. 6(a) and (b). Such a change is accompanied by the increase in $\bar{v}$ and ℓ. We propose that this is the origin of the observed increase in peak AE levels from 0.2 T_m to T_c. Above T_c, dislocation structures undergo dynamic recovery (and possibly recrystallization) and remain unchanged except for larger cell sizes at higher T_D. However, the phonon drag term B is expected to restrict v above T_c. Thus, overall temperature dependence of V_r can be given schematically by Fig. 7.

On the basis of the observed dislocation structures, another possible origin

of the AE behavior comes from the variation in the magnitude of slip steps. At higher T_D, the obstacles are stronger, but thermal activation can release a deeply trapped dislocation source. When $\Delta\epsilon^*$ is large, $\dot{N}$ becomes smaller [Eq. (4)]. From Eq. (5), this situation yields a higher V_r, which also may explain the observed temperature dependence.

CONCLUSIONS

This study examined test temperature effects on AE behavior of three pure metals, Cu, Aℓ and Fe. The peak AE levels showed a maximum at 0.3 to 0.4 T_m. The decay of AE level beyond the macroscopic yielding was related to work hardening parameter. A theoretical model of continuous emission was presented. Important features of AE behavior were discussed in terms of the model in conjunction with reported dislocation substructures.

ACKNOWLEDGEMENTS

This research was supported by the Physics Program, Office of Naval Research.

REFERENCES

1. Carpenter, S.H. and Heiple, C.R., Fundamentals of Acoustic Emission, K. Ono (ed.), Materials Department, UCLA, Los Angeles, 1979, p. 49.

2. Kishi, T. and Kuribayashi, K., Fundamentals of Acoustic Emission, K. Ono (ed.), Materials Department, UCLA, Los Angeles, 1979, p. 105.

3. Eisenblätter, J., Jax, P. and Schwalbe, H., "The Second Acoustic Emission Symposium," September 1974, Tokyo, Japan, Session, p. 1.

4. Malen, K. and Bolin, L., phys. stat. sol(b) 61 (1974) 637.

5. Ono, K., Fundamentals of Acoustic Emission, K. Ono (ed.), Materials Department, UCLA, Los Angeles, 1979, p. 167.

6. Hsu, S.-Y. S., Ph.D. Thesis, UCLA, 1980.

7. Kiesewetter, N. and Schiller, P., phys. stat. sol.(a) 38 (1976) 569.

8. Vreeland, T. (Jr.), Dislocation Dynamics, McGraw-Hill, New York, 1968, p. 529.

9. Turner, A.P.L. and Vreeland, T. (Jr.), Acta Met. 18 (1970) 1225.

10. Chen, H.S., Gilman, J.J., Head, A.K., J. Appl. Phys, 35 (1964) 2502.

11. Argon, A.S., Mat. Sci. Engr. 3 (1968/69) 24.

12. Kocks, U.F., Argon, A.S., Ashby, M.F., Thermodynamics and Kinetics of Slip, Pergamon Press, 19 (1975) 1.

13. Fujita, H. and Tabata, T., Acta Met. 21 (1973) 355.

14. Staker, M.R. and Holt, D.L., Acta Met. 20 (1972) 569.

15. Embury, J.D., Strengthening Methods in Crystals, A. Kelly and R.B. Nicholson (eds.), Halsted Press, New York, 1971, Chap. 6, p. 331.

16. Spitzig, W., Keh, A., Acta Met. 18 (1970) 61.

17. Keh, A.S., Spitzig, W., Nakada, Y., Phil. Mag. 23 (1971) 829.

18. Pharr, G.M. and Nix, W.D., Acta Met. 27 (1979) 433.

ACOUSTIC EMISSION OF PLASTIC FLOW - II. ALLOYS*

S.-Y. S. Hsu and K. Ono
Materials Science and Engineering
School of Engineering and Applied Science
University of California
Los Angeles, California 90024

ABSTRACT

This paper reports the second part of a comprehensive study on acoustic emission (AE) of plastic flow. AE behavior of eight different metallic alloys has been determined with the test temperature and heat treatment as the major variables.

The extent of solute segregation is the major factor determining the AE behavior in Cu-10 Ni, Cu-30Ni, Cu-10Zn and Cu-15Zn alloys. Solute concentration had minor effects when solute atoms were randomly distributed, and the AE output levels were similar to that in pure Cu. Higher alloying content increased the AE level strongly when solute segregation to dislocations was allowed. This is due to the emission arising from dislocation breakaway.

The AE output level of Ni-22Fe and its reponse to heat treatment and test temperature were significantly different from those in Cu-Ni alloys. The behavior cannot be attributed to the difference in SFE, but can be rationalized from the probable effect of the pinning due to short-range ordering. This is supported by similar results from Cu-30Zn, Cu-40Zn and Cu-7.5 Aℓ alloys.

These findings will be discussed in terms of the AE model developed in a preceding paper. It will be demonstrated that AE is a powerful probe to dislocation dynamics.

INTRODUCTION

Effects of solute atoms on mechanical properties of metallic alloys have been studied extensively. In addition to the change of stacking fault energy, solute atoms decrease the dislocation mobility via either solute pinning effect or solute frictional effect.[1,2] Since AE has proven its usefulness in probing the dislocation behavior during plastic deformation, the application of AE technique to the deformation of solid solution alloys should lead to a better understanding of the roles of solute atoms in solids. Such possibilities are investigated here, as no systematic study has been made.

We determined the AE behavior while deforming annealed specimens at different test temperatures, ranging from 300°K to 1173°K. The variation of the deformation temperature (T_D) is expected to affect the mode of dislocation glide, dynamic recovery and recrystallization, and the ability of solute atoms to interact with glide dislocations. Eight different alloys were tested,

*Supported by the U.S. Office of Naval Research, Physics Program.

including two Cu-Ni alloys (10 and 30 wt.% Ni), four Cu-Zn alloys (10, 15, 30 and 40 wt.% Zn), Cu-7.5 wt.% Aℓ and Ni-22% Fe. In the following, representative AE behavior will be presented and possible mechanisms outlined. Detailed experimental results and discussions will be described elsewhere.[3] The experimental set up was the same as that for pure metals described in the previous paper.

EXPERIMENTAL RESULTS

The AE behavior of eight alloys studied here can be separated into two groups. Group I includes Cu-10Ni, Cu-30Ni, Cu-10Zn and Cu-15Zn. The changes of the characteristics of the rms voltage, V_r vs. strain curves with T_D of Group I alloys, represented by Cu-10Ni and Cu-30Ni, are shown in Figs. 1 and 2. In Cu-10Ni, simple V_r-strain curves, typical to those of pure Aℓ or Cu, were observed below 673°K. At 673°K and 773°K, fluctuations in AE outputs emerged after 8% and 2% plastic strain, respectively.

Fluctuations almost disappeared at 873°K, and V_r was reduced to almost the background level after a few percent plastic strain. The peak AE output near macroscopic yielding varied with T_D and exhibited a maximum value at T_C of 650°K, as shown in Fig. 3(a). This T_C corresponds to 0.4 T_m (T_m = 1420°K) and is slightly higher than T_C for Cu.[4] In Cu-30Ni, fluctuations were again observed at 673°K and 773°K. The fluctuations at 773°K were more pronounced in magnitude and started closer to the macroscopic yielding. At 873°K and 953°K, the shape of the AE peak at yielding became narrow, i.e., faster drop of V_r after reaching the peak. This was followed by a near constant signal level with further deformation. The increase of V_r at peak AE output from 300°K to T_C (= 770°K, or 0.51 T_m) was 70 μV larger than that in Cu-10Ni. This is shown in Fig. 3(b).

Group II includes Cu-30Zn, Cu-40Zn, Cu-7.5Aℓ and Ni-22Fe. Characteristic V_r-strain curves of Group II alloys, represented by Ni-22Fe here, are shown in Fig. 4. We found the following features, which were significantly different from Group I alloys:

i) Peak AE output was high (120 μV) at 300°K and further increased with increasing temperatures up to 1073°K, where it was nearly three times higher. At 1173°K, however, the peak value decreased drastically to about 35 μV.

ii) AE behavior near macroscopic yielding showed different peaking behavior. Immediately after the maximum output signal was observed, AE level dropped rapidly to much lower levels. At T_D below 873°K, AE peaks also contained many spikes.

iii) At 673°K, strong fluctuations of AE level of the order of 50 μV were detected. These were also found at 773°K, but the characteristics of the fluctuation differed with much shorter duration and larger magnitude of over 100 μV. These large fluctuations at 773°K were not observed in Cu-Ni alloys or stainless steels.[5]

iv) Strong second AE peaks were observed at 873°K and 973°K. These peaks were quite broad. The strains at which the second peak reached its maximum AE output level were about 15% at 873°K and 6% at 973°K, respectively.

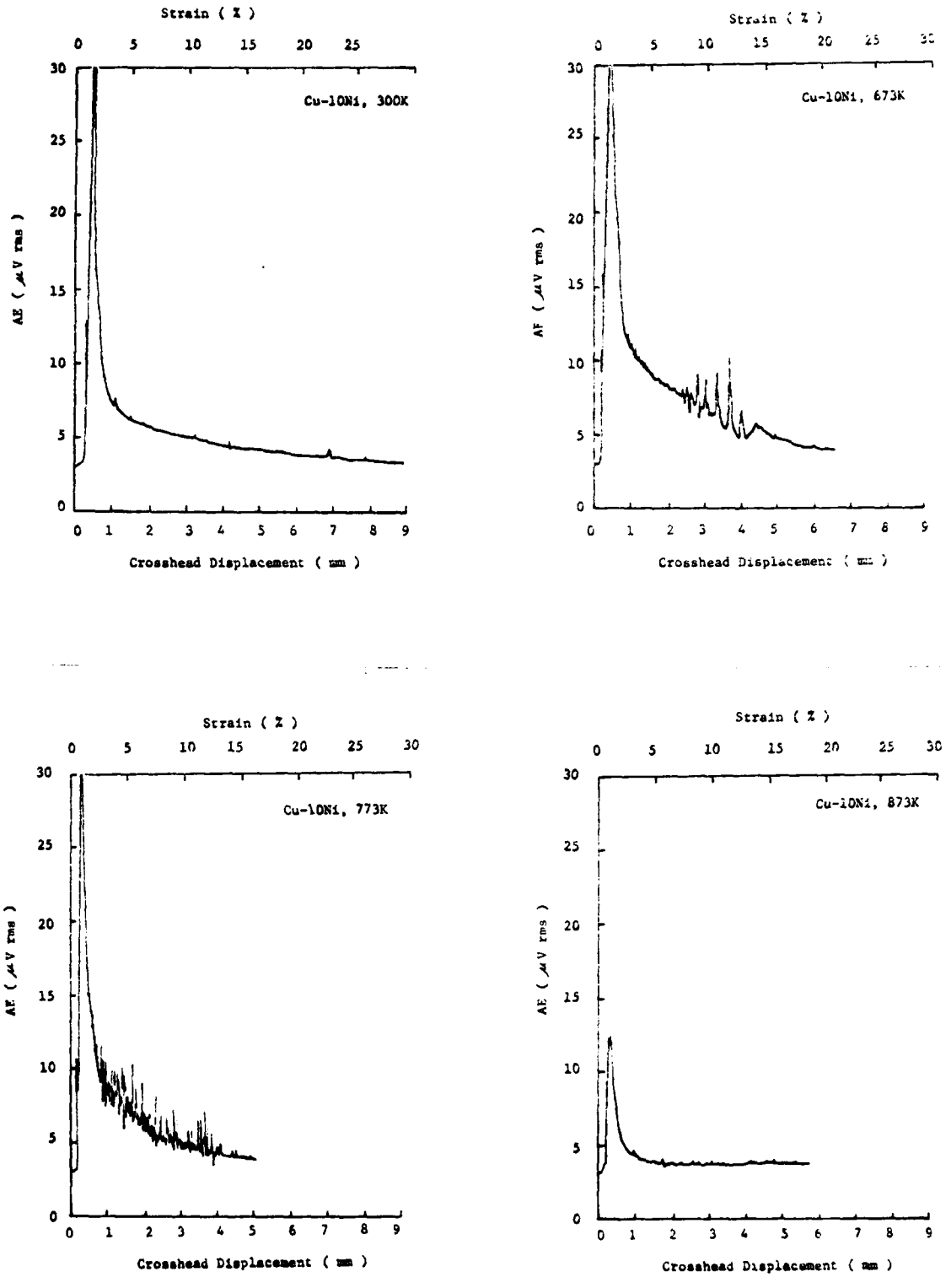

Fig. 1 Effects of temperatures on the V_p-strain curves of Cu-10 Ni.

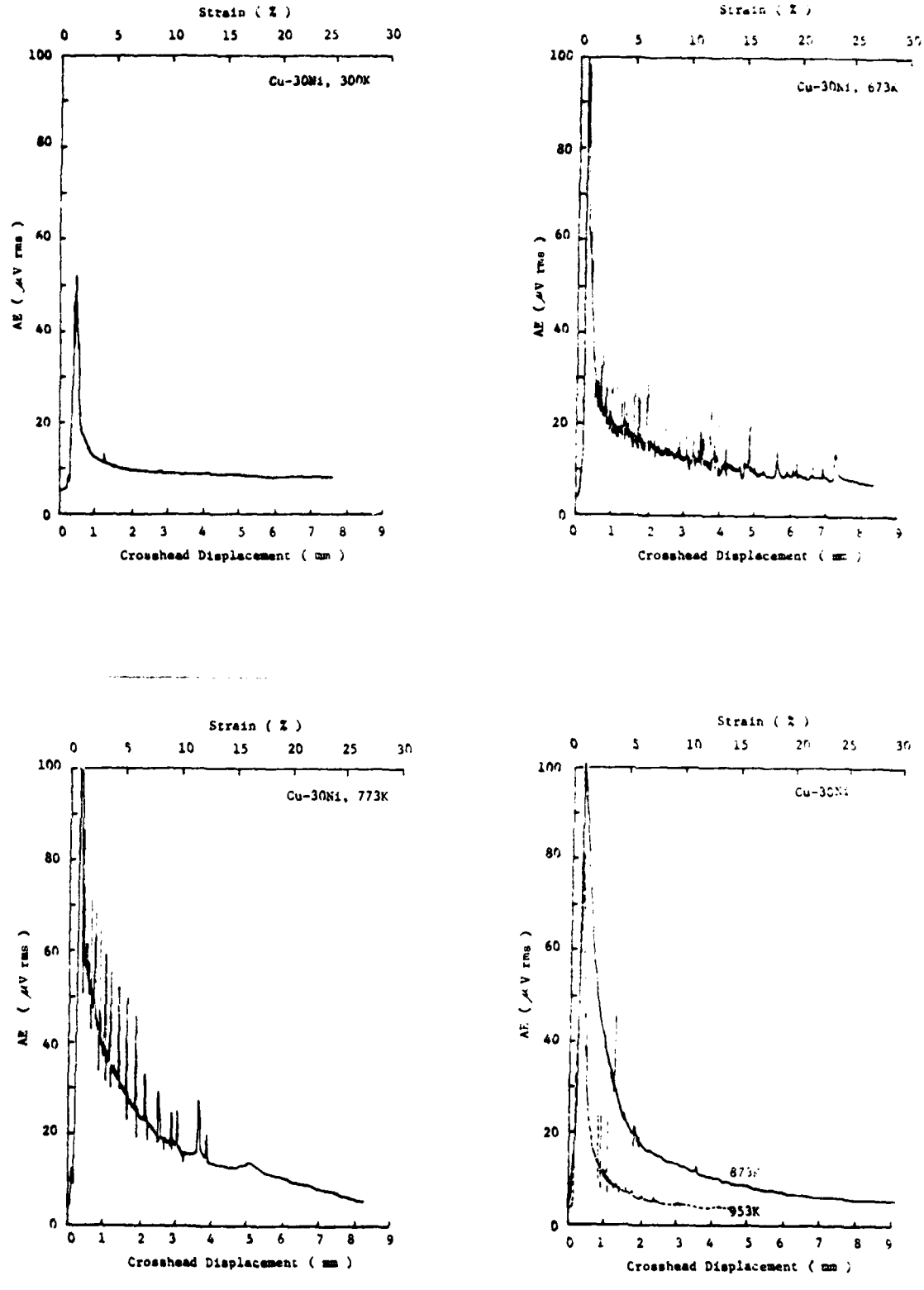

Fig. 2 Effects of temperatures on the V_r-strain curves of Cu-30 Ni.

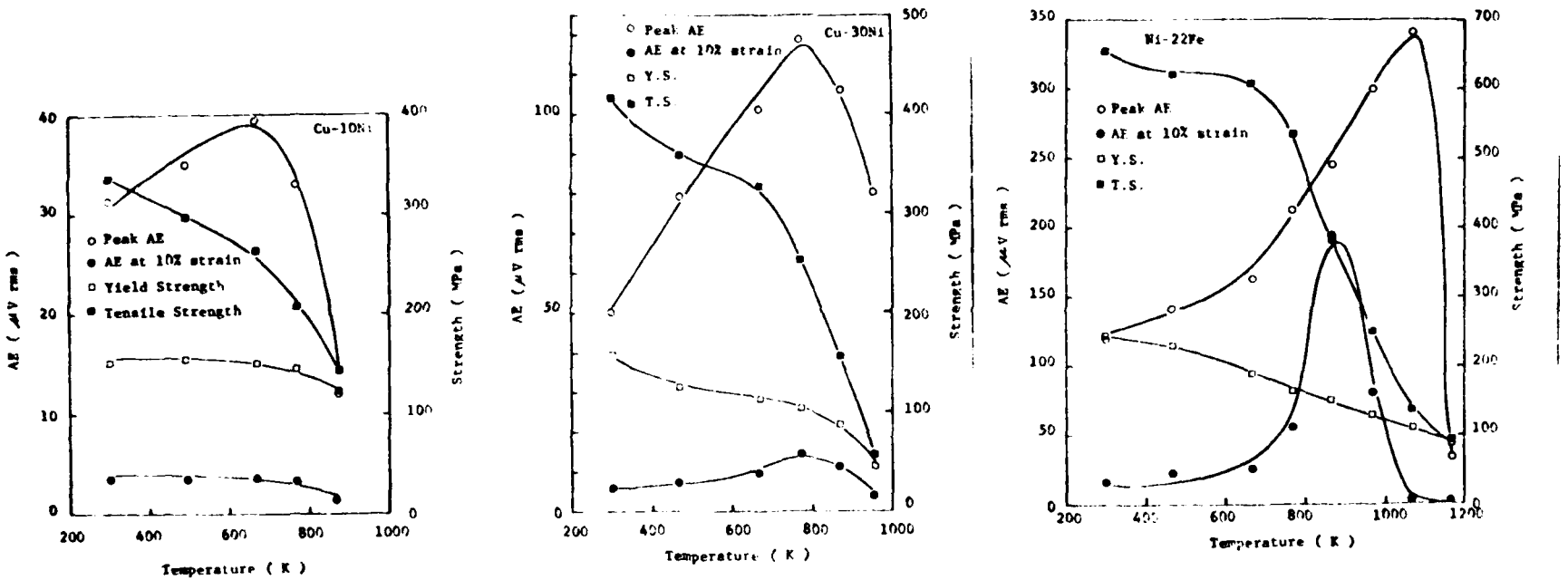

Fig. 3 Effects of temperatures on the AE output levels and mechanical properties of Cu-10 Ni, Cu-30Ni and Ni-22Fe.

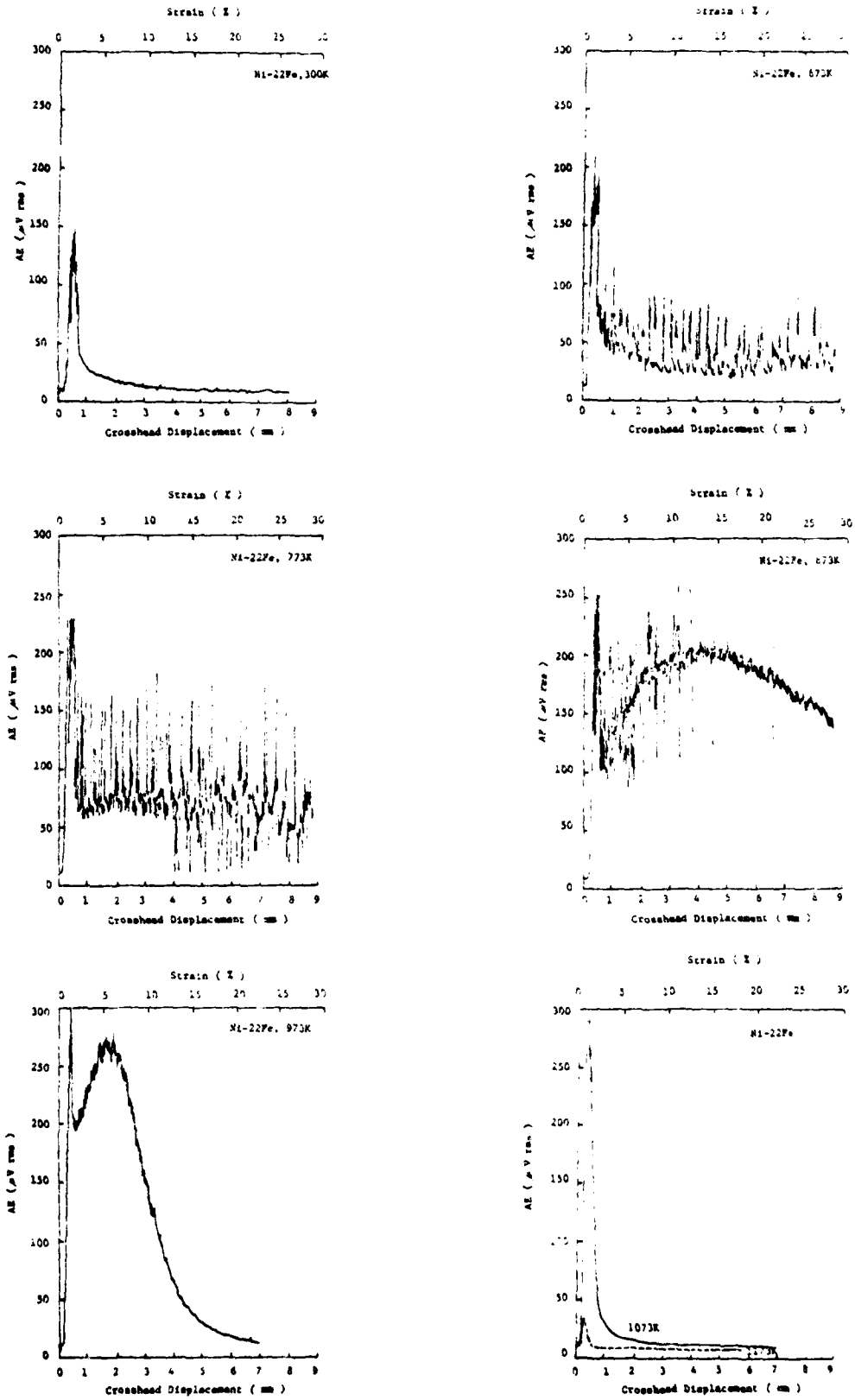

Fig. 4 Effects of temperatures on the V_r-strain curves of Ni-22 Fe

v) As shown in Fig. 3(c), the maximum in peak AE level was reached at T_c of 1073°K, or, 0.63 T_m. This was higher than T_c of 0.51 T_m for Cu-30Ni.

vi) Due to the emergence of the second AE peak, V_r at 10% strain increased sharply at T_D of 873°K [Fig. 3(c)]. It was reduced to less than 10 μV at 1073°K and above. Unlike Cu-Ni alloys, the temperature corresponding to the maximum AE output at 10% strain in Ni-22Fe was about 200°K lower than T_c.

In Fig. 5, the temperature dependence of peak AE output near macroscopic yielding for both Group I and Group II alloys are plotted as the function of homologous temperature. The solid lines represent the original data while the dashed lines have been corrected for experimentally determined attenuation effects at elevated temperatures. The temperature corresponding to the maximum AE output was always lower than 0.6 T_m for Group I alloys. The observed increase of AE output from 300°K to T_c were also much smaller in Group I alloys than in Group II alloys. In Group II alloys, T_c was above 0.63 T_m (except Cu-7.5Aℓ), and AE output levels decreased sharply above T_c.

DISCUSSION

As has been discussed in the previous paper,[4] pure Aℓ or Cu had AE output levels in the range of 10 to 20 μV near macroscopic yielding. For annealed samples, Cu-Ni alloys at 300°K had AE output of 30 μV for Cu-10Ni and 50 μV for Cu-30Ni. Such an increase of AE due to solute addition can be attributed to the solute segregation. Solute segregations around dislocations produce a pinning effect, locking existing dislocations. When the applied stress becomes high enough to overcome the binding energy between the segregated solute atoms and dislocations, dislocations break away from the pinning atmospheres and multiply themselves. As they spread, stress pulses are radiated outward due to the accelerated motion of dislocations. The AE output signals are shown to be related to the solute-dislocation binding force σ_o by

$$V_r \alpha \frac{\sigma_{ob}}{B} \cdot \sqrt{\dot{N}} \qquad (1)$$

where b is the Burgers vector, B is the dislocation drag coefficient and $\dot{N}$ is the rate of dislocation unpinning. σ_o, which increases with solute concentration [6] is apparently responsible for the observed increase of V_r.

Experimentally, the effect of solute segregation at dislocations can be eliminated by quenching alloy samples from elevated temperatures, where the entropy contribution overcomes the reduction of the free energy due to the solute segregation. Observed AE levels were almost identical among Cu and quenched Cu-Ni alloys, when the quenching temperature was above 900°K. This observation clearly demonstrates the solute effect on AE to be due to the solute atmosphere at dislocations. Moreover, it implies that the drag coefficient has no direct effect on V_r when the solute concentration is increased. In our previous study[5] on low stacking fault energy (SFE) alloys (stainless steels, AISI 304L and 316), we found that planar dislocation glide reduced the AE output. In Cu-Ni alloys, this effect appears to be absent as SFE is not lowered significantly by Ni additions.

The variations of the AE output level with deformation temperature were about 10 μV in pure Aℓ or Cu. In Cu-Ni alloys, the increases were larger, especially in Cu-30Ni. Since the AE fluctuations in Cu-30Ni occurred close to

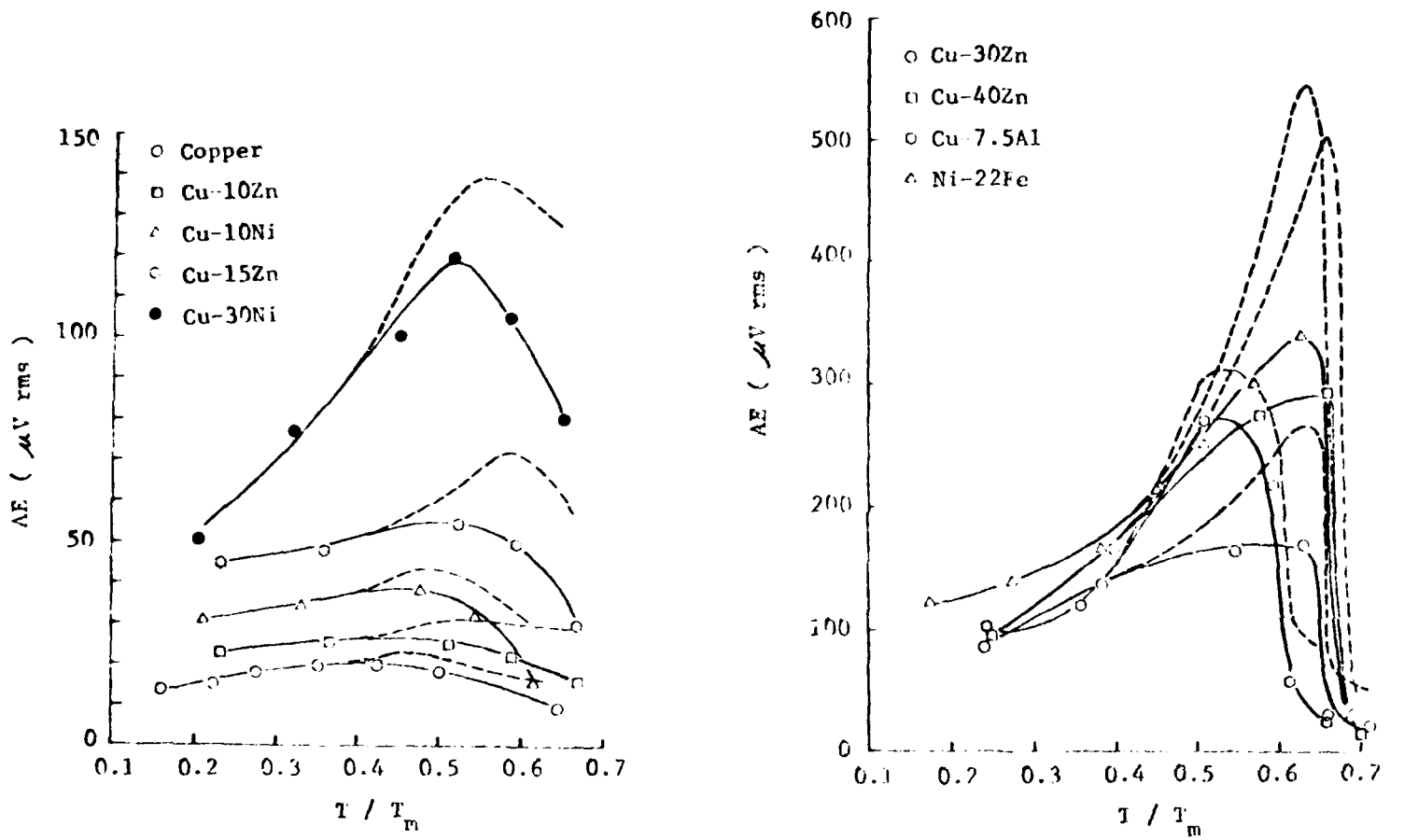

Fig. 5 Variations of peak AE output levels in Group I and Group II alloys with homologous temperatures. Dash lines represent the AE output levles after the correction for elastic wave attenuation.

the macroscopic yielding at 773°K, the larger increase of peak AE output in this material was in part due to the effect of dynamic strain aging. However, the major part is believed to arise from the intrinsic nature of solute pinning since similarly a large increase was observed in nickel where carbon atmospheres were known to be active.[3] It is expected that the temperature dependence is partially due to the same mechanisms as in pure metals; that is, the variations in dislocation substructures and phonon drag force. The effect of SFE can be discounted as no major change of glide mode has been observed in Cu-Ni alloys.

The AE behavior of Ni-22Fe was significantly different from that in Cu-Ni alloys. Solute segregation effect alone cannot explain such difference, because the solute concentration of Ni-22Fe is lower than in Cu-30Ni and the atomic misfit between solute and solvent atoms is smaller in Ni-Fe alloys. However, short-range ordering (SRO) has been found to exist in Ni-Fe alloys with compositions near Ni_3Fe.[7,8,9] Since SRO produces both locking effect[10] and frictional effect[11-13] on dislocations, the dislocation behavior is affected by SRO. The peculiar slip patterns observed in alloys with SRO[12] is an example of the change in the dislocation behavior. SRO has also been confirmed to exist in other materials of Group II alloys, either directly or indirectly.[12] Therefore, the existence of SRO is suggested as the cause of the observed differences in AE behavior between Group I and Group II alloys. Other experimental findings due to heat treatment also revealed the differences between these two groups of alloys, and can be explained in terms of solute segregation and SRO effects.[3]

The yield strength of Ni-22Fe and other Group II alloys was affected little by the presence of SRO, as the results of quenching experiments indicated. The observed temperature dependence of the yield strength also showed no peculiar behavior near T_c. However, rapid decreases of the tensile strength, coincided with the sharp decrease of AE at 10% strain, as shown in Fig. 3(c). Although substantial SRO is maintained to over 1000°K in Ni-22Fe, the degree of SRO should be weakened at temperature increases above 900°K according to the quenching and diffraction experiments.[3,14] The peak AE level, however, reached the maximum at 1073°K. This increase in the AE level cannot be explained by stronger SRO. As in the case of unpinning induced AE in Ni-C alloys,[3] we expect higher AE levels originating from the overcoming of deeply pinned dislocation sources, which contributes to larger instantaneous plastic strain increments. This is attributed to stronger thermal activation at higher deformation temperatures.

Rapid reduction in the peak AE levels above T_c cannot be due to the change in SRO, which decreases gradually with temperature.[3,14] This behavior is common to other Group II alloys as well.[12] Another possible explanation is the absence of preferential SRO at dislocations above T_c. However, this can be ruled out, because the AE level increased gradually during the quenching experiment below 1200°K through the T_c range. It thus appears that the rapid reduction above T_c can be attributed to the absence of pinning by SRO, stemming from high diffusion rates of solute atoms at temperatures above T_c. This further implies that pinning effect of SRO is the source of high AE outputs in Group II alloys.

Finally, we should note the AE behavior of commercial aluminum alloys as a function of deformation temperature. In 7075 and 7049 alloys, the AE level of the so-called second peak decreased with increasing T_D. This peak originates from the fracture of insoluble second-phase particles and the observed reduction is interpreted to be due to the loss of thermal misfit stress, which contributes to lower AE levels.[3]

CONCLUSIONS

A comprehensive study of AE behavior in a wide variety of alloys has revealed the solute segregation to dislocations and the preferential SRO at dislocations to be the sources of strong AE responses in Group I and II alloys, respectively. Frictional forces of randomly distributed solute atoms have hardly any contribution to AE when the glide mode remains unchanged. This is in sharp contrast to AE in stainless steels, where a low SFE leads to low AE levels. A few other sources of AE behavior have been identified in this study.

REFERENCES

1. Haasen, P., Physical Metallurgy, R.W. Cahn (ed.), 2nd edition, North-Holland, 1970, Chapter 17, p. 1011.

2. Nabarro, F.R.N., The Physics of Metals, P.B. Hirsch (ed), Part 2, Cambridge University Press, 1975, Chapter 4, p. 152.

3. Hsu, S.-Y. S., Ph.D. Dissertation, University of California, Los Angeles, 1980.

4. Hsu, S.-Y. S., and Ono, K., this volume.

5. Hsu, S.-Y. S., Ono, K. and Hatano, H., Materials Science and Engineering, 38 (1979) 187.

6. Suzuki, H., Dislocations and Mechanical Properties of Crystals, J.C. Fisher, et al., Wiley, New York, 1957, p. 361.

7. Calvayrac, Y. and Fayard, M., phys. stat. sol.(a), 17 (1973) 407.

8. Victoria, M. and Vidoz, A.E., phy. stat. sol., 28 (1968) 131.

9. Vidoz, A.E., Lazavević, D. and Cahn, R.W., J. Phys. Society, Japan, 18 Suppl. 1 (1963) 24.

10. Sumino, K., Science Report Research Institute, Tokyo University, 1958, A10 (1958) 283.

11. Fisher, J.C., Acta Met., 2 (1954) 9.

12. Cahn, R.W., "Local Atomic Arrangements Studied by X-ray," AIME, 1965, p. 1979.

13. Cohen, J.B. and Fine, M.E., Journal De. Phys., Radium, 23 (1962) 749.

14. Lefebvre, S., Bley, H, Bessiere, M., Fayard, M., Roth, M. and Cohen, J.B., AIP Conference Proceedings No. 53, "Modulated Structures 1979," J.M. Cawley, et al., American Institute of Physics, New York, 1979, p. 286.

THE DIRECTIONAL PROPERTIES OF HSLA STEELS DURING ACOUSTIC EMISSION AND FRACTURE TESTING

M. Yamamoto
Sumitomo Heavy Industries, Ltd.
Hiratsuka, Japan

and

C. Ouchi
Nippon Kokan K.K.
Kawasaki, Japan

and

K. Ono
Materials Science and Engineering Department
School of Engineering and Applied Science, U.C.L.A.
Los Angeles, California U.S.A. 90024

ABSTRACT

Effects of nonmetallic inclusions on the ductility, fracture toughness and AE behavior are well-known. Flattened MnS inclusions form during hot rolling operation and cause these deleterious effects. Our previous studies revealed clear anisotropic AE behavior during tensile testing originating from the particular morphological features of MnS inclusions.

In the present study, the effects of number, size and shape of manganese sulfide inclusions on the energy absorbed in Charpy impact testing and AE behavior during Charpy 3 point slow bend test have been investigated. The size and the shape of manganese sulfide inclusions were controlled by changing rolling ratio and finish roll temperature.

Results show the energy absorbed decreased greatly, when material was heavily rolled except in LS oriented specimen. In LS specimen, the energy absorbed increased with increasing rolling ratio and the number of inclusions. In the AE studies, undeformed material showed no anisotropic AE behavior. Anisotropy of AE signals was observed in the hot rolled material, and the AE activities increased with increasing rolling ratio.

The results of fracture and AE studies will be correlated to metallographic measurements, scanning electron microscopic observations and the conditions of metal processing. The roles of internal stresses on the inclusion debonding process will be discussed in conjunction with the stress field at the tip of the crack.

I. INTRODUCTION

Acoustic emission (AE) from structural steels has been investigated extensively. See References 1 and 2 for a comprehensive listing of these studies. Many possible sources of observed AE signals have been suggested. These include i) dislocation motion,[3-5] ii) cleavage cracking,[6,7] iii) void coalescence,[6-9] iv) carbide cracking,[4,10] v) the cracking of cementite in pearlite,[4,10,11] vi) the rapid shear linkage of growing voids,[12] vii) grain boundary cracking,[7,13] viii) the fracture of nonmetallic inclusions[14] and ix) the debonding (decohesion) of nonmetallic inclusions, especially manganese sulfide (MnS) inclusions.[1,15-19]

Anisotropic AE behavior and its strong dependence on the sulfur content of low alloy steels have revealed the importance of MnS inclusions as the source of burst-type AE.[15-17] The MnS inclusions are flattened into ribbon shapes during hot rolling.[20-23] The broad faces of the inclusions are weakly bonded to the steel matrix and readily separate under tensile stress. AE signals due to the debonding possess a characteristic amplitude distribution, which has been correlated to the size distribution of MnS inclusions via a theory of AE signal generation.[17,24]

It is well known that the ductility and fracture toughness of a steel plate is strongly affected by nonmetallic inclusions, MnS in particular.[20-23] Presently, various methods of desulfuridation and sulfide shape control are adopted to reduce the deleterious effects of MnS. In order to clarify the roles of MnS in reducing the ductility and in generating AE signals, we have investigated anisotropic AE behavior of two thick plates of ASTM A533B steels.[1] The sulfur content of the two plates were 0.005% and 0.021%. From the types of AE signals, AE event counts, signal levels and amplitude distribution, three distinct AE characteristics were identified. When the direction of uniaxial tensile stress or that of crack propagation favored the debonding of MnS inclusions, burst AE with the characteristic amplitude distribution function was observed. Continuous-type AE was observed when the plastic deformation was primarily expected. In this case, the third type of AE signals with a power law amplitude distribution was also found simultaneously. Generally speaking, higher burst AE activities correlated to lower fracture resistance as measured by the absorbed energy during the slow bend Charpy tests. However, crack blunting by MnS inclusions increased the absorbed energy values in some orientations. The observed orientation and sulfur content dependencies were shown to arise from the difference in the number of MnS inclusions with a certain normal stress on their broad faces.

In the present study, we attempt to verify the observed effects of MnS on the fracture and AE behaviors of another low alloy steel, JIS SM50. Sulfur content is varied and the directionality effects are examined. In addition, the shape and size of MnS inclusion are varied by changing the rolling ratio and finish rolling temperature. Results on SM50 steel again manifest the consequences of the inclusion debonding model and confirm the validity of a conclusion of the A533B steel study; i.e., burst-type AE in most fracture/AE testing of a ductile structural steel originates primarily from the debonding of nonmetallic inclusions.

II. MATERIALS AND EXPERIMENTAL PROCEDURES

Two heats of JIS SM50 steel were used in this study. The chemical compositions are given in Table 1.

Table 1. Chemical Composition

	C	Si	Mn	P	S	Cu	Cr	Ni	Nb	Al
Slab A	0.17	0.34	1.29	0.016	0.019	0.01	0.02	0.01	0.019	0.029
Slab B	0.15	0.29	1.33	0.019	0.006	0.03	0.02	0.02	0.024	0.020

om Slab A of 160 mm thickness, three steel plates were obtained; T-1, without ditional rolling, T-2 after 25% reduction to 120 mm thickness and T-3 after % reduction to 25 mm thickness. Plates T-4 and T-5 were obtained from Slab B, ich was rolled from 190 mm to 25 mm thickness. The finish roll temerature for ates T-2, T-3 and T-4 was 1273K, whereas that for T-5 was 1023K. The initial ll temperature was always 1473K. All the materials were normalized at 1173K r 1 hr. These plates are the same as those used in a previous AE study.[17]

Standard V-notch Charpy specimens were machined from the five steel plates. x possible directions were used as shown in Fig. 1, which also shows hematically the orientation of MnS inclusions in a rolled plate. Here, L,T d S refer to the longitudinal (rolling), long-transverse and short-transverse hickness) directions. For Charpy samples, the first letter indicates the ress direction and the second direction of crack propagation. For SL and ST mples of T-3 4 and 5 plates, effective plate thickness was first increased by lding two steel plates on both surfaces of 25 mm thick sample material.

All the mechanical tests were performed at room temperature. Charpy impact sting was conducted conventionally without any fatigue precracking. For AE sts, 1 mm long fatigue precrack was introduced. AE data was obtained during ow bend Charpy tests on a floor-model Instron at a constant crosshead speed of 021 mm/s. Three pins, 6.35 mm diameter, were used with the span of 40 mm. ie loading points were prestressed to 18 kN to eliminate spurious noise. The ontact points were also lubricated by STP oil additive.

AE characteristics evaluated were totalized AE event counts, rms voltages id the peak amplitude distribution of AE signals. A resonant type transducer fodel AC 175L, Acoustic Emission Technology Corporation (AET), Sacramento, alifornia) and a preamplifier with 125-250 kHz filter (Model 160, AET) were sed for all AE measurements. For AE event count measurements and the amplitude stribution analysis, an amplitude distribution analyzer (Model 203, AET) was ployed. A true rms voltmeter (Model 3400A, Hewlett-Packard) was used for the is voltage measurements. The input noise level was 1.4 μV and the threshold or amplitude distribution analyzer was set at 10 mV after 60 dB amplification or 10 μV in reference to the preamplifier input). When only the event counts ere measured in separate tests, the threshold value was set at 40 mV in order o eliminate the contributions from continuous-type AE. The transducer was onded to the end of a Charpy specimen with bees wax (Model SC1, AET).

During a test, cumulative AE event counts, rms voltages and load were ecorded continuously on two 2-pen recorders. The cumulative amplitude stribution of AE signals was photographed at several selected points during ie test. Immediately after the photographic recording, the display of the plitude distribution analyzer was reset. Note that this part of the analyzer s independent of the totalizing function of AE event counts. Each amplitude stribution data represented those AE signals between the photographic ecordings, which were marked on the load-time curve. The loss of AE data due o resetting was negligible.

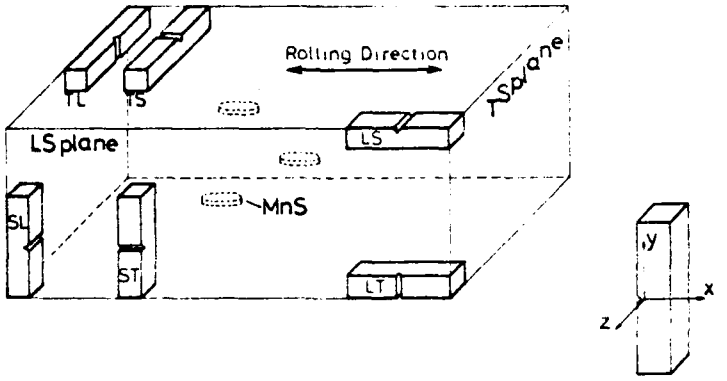

Fig. 1 Specimen orientations relative to the rolling direction. Flattened manganese sulfide inclusions are schematically shown with elliptical discs (dotted lines).

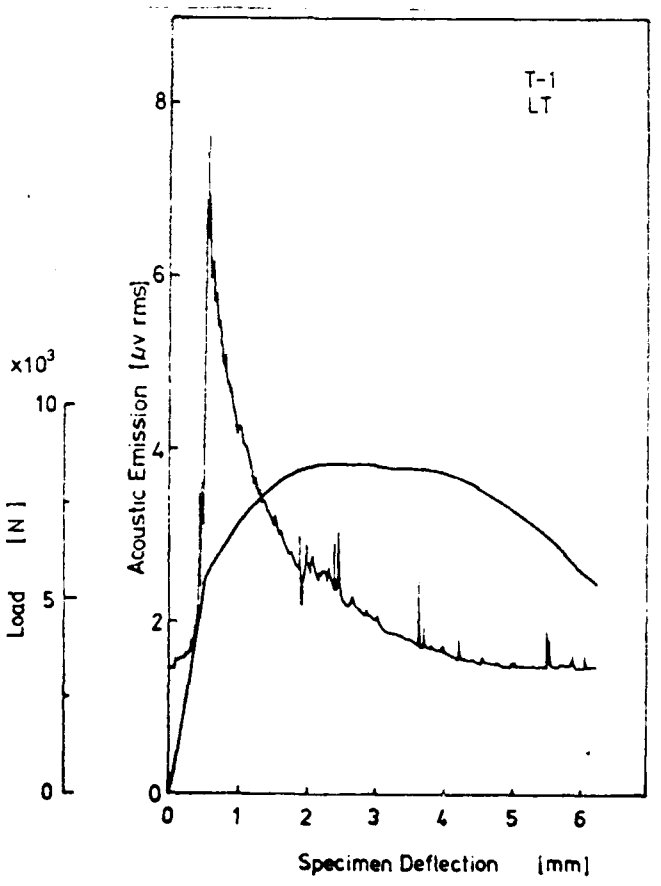

Fig. 2 Stress and AE level against specimen deflection for Charpy slow bend test in LT specimen to T-1 steel.

III. RESULTS

1. Charpy Impact Tests

The absorbed energies, E_a, of Charpy impact tests are tabulated in Table 2. The value ranged from 25 J to 272 J. For a given plate, E_a can be grouped according to the stress direction; LT and LS, TL and TS and SL and ST, respectively. Within each of the groups, E_a values for the LS and TS orientations were slightly higher than those for the LT and TL orientations. One significant exception was for T-3 plate samples; E_a for the LS orientation was nearly twice that for the LT orientation.

E_a values for T-1 and T-2 plates were essentially identical to each other for a given orientation. For the second and third groups, those for T-3 plates were significantly reduced in comparison to T-1 and T-2 plates. On the other hand, E_a was higher for the LS and lower for the LT orientation in T-3 plate. The ratio of maximum to minimum E_a values was 3 for T-1 plate and was 7 for T-3 plate, indicating a large increase in the anisotropy of E_a with increasing severity of hot rolling operation.

E_a results for T-4 and T-5 plates were comparable. This implies that effects of the finish roll temperature were not apparent in these tests. It is interesting to note that the elongation and reduction in area of the thickness direction tensile tests revealed deleterious effects of a lower finish roll temperature.

When results of T-3 and T-4 plates are compared, the reduced sulfur content yielded higher E_a valuesin T-4 plate, especially in the transverse (TL, TS) and thickness (SL, ST) orientations. As a consequence, the anisotropy in E_a was nearly halved from 7 to 4.

2. AE Behavior

Load and the rms voltage of AE signals during slow bend Charpy testing are plotted against deflection in Fig. 2. Figure 2 shows the results for the LT orientation of T-1 plate, which exhibited the lowest AE activities among 30 sets of samples (five plate,six orientations). AE activities started at the precrack load of 3 kN and peaked at the general yield, followed by a decrease in the rms voltage level. These general trends in the rms voltage curve were accompanied by occasional spikes. Eight of these were found at the deflections between 1.8 mm and 6mm and were apparently caused by the motion of the loading contact pins, judging from long pulse durations of the signal waveforms. This AE behavior is typical for the other five orientations of T-1 plate. It is dominated by continuous type AE signals.

Cumulative AE event counts vs. specimen deflection data for all the orientations of T-1 plate are shown in Fig. 3. Notice that virtually no orientation dependence existed and that most events occurred near the general yield. Total event counts were also low (120-200). Since the threshold level was deliberately set to eliminate effects of continuous AE, Fig. 3 represents the contribution of only high amplitude burst AE (with peak amplitude greater than 40 μV).

The dominance of continuous AE is further demonstrated in Figs. 4 and 5, which show the cumulative peak amplitude distribution against peak amplitude for the LT and ST samples of T-1 plate. The circles on the attached load-deflection curves indicate the positions, at which the particular amplitude distribution was measured. These distribution curves above the peak amplitude of 30 to 34 μV

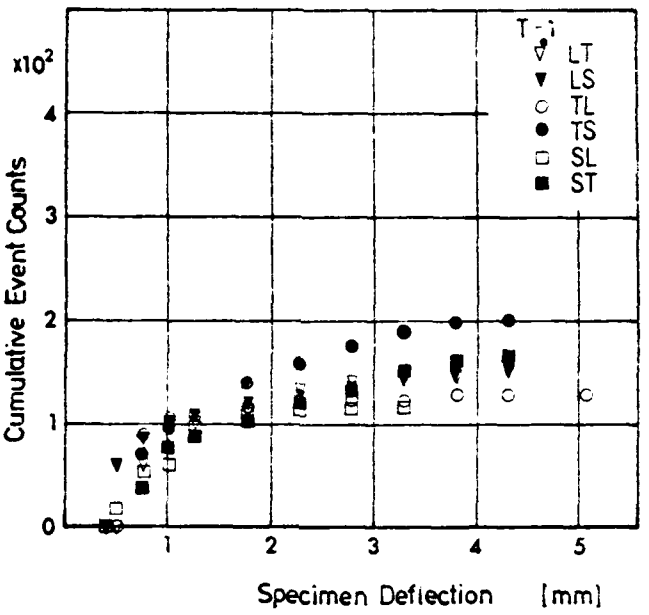

Fig. 3 Cumulative AE event counts against specimen deflection for Charpy slow bend tests in T-1 steel.

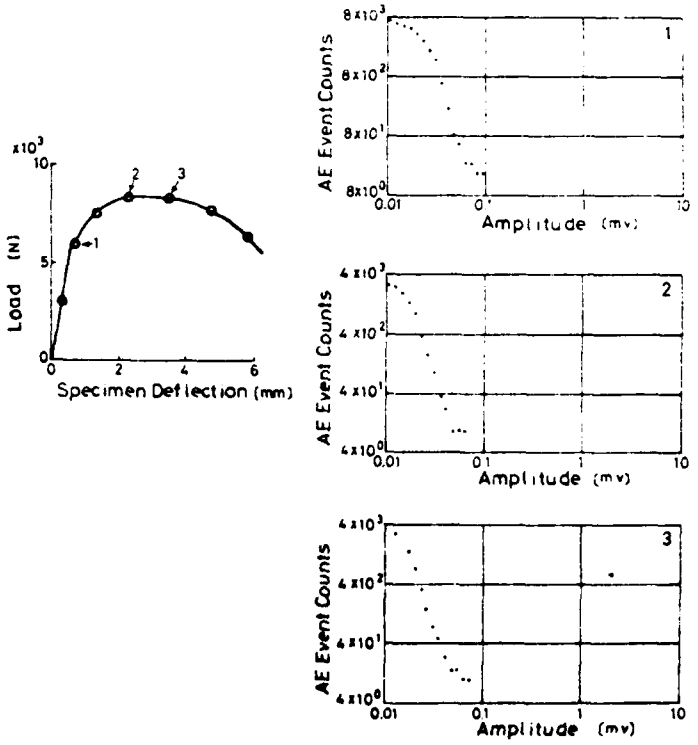

Fig. 4 Cumulative amplitude distributions of AE events during Charpy slow bend test in LT specimen of T-1 steel. Load-deflection curve also shown.

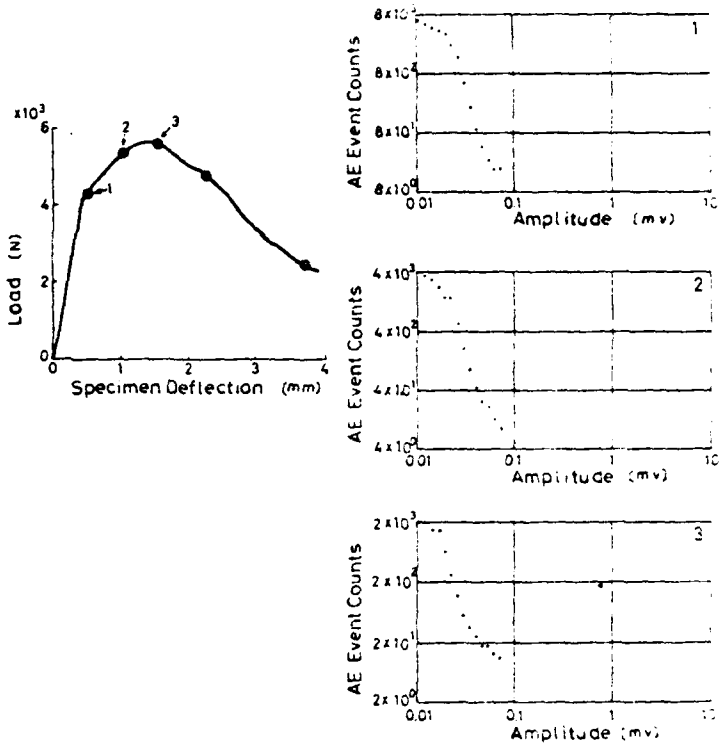

Fig. 5 Cumulative amplitude distributions of AE events during Charpy slow bend test in ST specimen of T-1 steel. Load-deflection curve also shown.

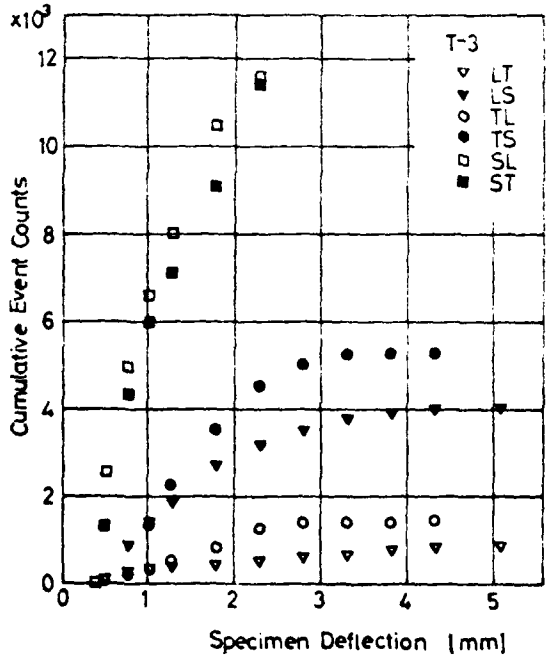

Fig. 6 Cumulative AE event counts against specimen deflection for Charpy slow bend tests in T-3 steels.

can be fitted to the usual power-law form,[6,24]

$$F_1(V_p) = A\, V_p^{-n} \qquad (1)$$

where F_1 is the cumulative event amplitude distribution function, V_p is the peak amplitude, n is the exponent and A is a constant, respectively.

The highly amplitude dependent part below V_p of 30 to 40 μV is apparently due to continuous type AE signals. As previously demonstrated, this amplitude distribution function, F_2, obeys a Weibull distribution of the form[17,26]

$$F_2(V_p) = B \exp\,(-B' V_p^4), \qquad (2)$$

where B and B' are constants. Note that the Gaussian distribution corresponds to Eq. (2) with the exponent 2.[27] This difference in the exponents was a consequence of the particular signal processing method employed in the analyzer.

It should be noted here that the continuous AE signals observed during yielding originate from the motion of dislocations.[28,29] Whereas no exact mechanisms of AE generation have been established, it is generally agreed that the rapid multiplication and propagation of glide dislocations across a grain are involved. When the continuous AE contributions are subtracted, the remaining event counts were about 140 for both the LT and ST samples (Figs. 4 and 5) in good agreement with those found in Fig. 3.

In the LT and TL orientations, AE behavior of T-2 plate samples was similar to that of T-1 plate. The rms voltage curves of T-2 plate samples contained more spikes, but generally resembled those of T-1 samples. However, as can be seen in Table 3, more high amplitude burst emissions were observed in the other four orientations, the SL and ST orientations in particular. In Table 3, cumulative AE event counts at the deflection of 2.54 mm, N_e^*, are summarized. This value of deflection was chosen as the burst emissions were less active and more spurious noise tended to occur at larger values of deflection. T-2 plate samples increased almost ten-fold in the SL and ST orientations over those of T-1 plate. Since the LT orientation of T-2 plate showed a decrease in N_e^*, the ratio of AE event counts, $R_e = N_e^*(ST)/ N_e^*(LT)$, became 24 in the T-2 plate in sharp contrast to unity in the T-1 plate.

AE behavior of T-3 plate samples was similarly anisotropic as shown in Fig. 6. Cumulative AE event counts for the six orientations are plotted against specimen deflection. The SL orientation was most active and the LT least. Clearly, the data can be classified into three groups. In order of AE activities, Group A includes the ST and ST, Group B TS and LS and Group C TL and LT, respectively. These groupings are common in T-2, T-3, T-4 and T-5 plates as well as the two plates of A533B investigated previously.[1] The values of N_e^* in T-3 samples were about ten-times larger than those of corresponding T-2 samples (see Table 3). The anisotropy as indicated by the event count ratio R_e was comparable between T-2 and T-3 plates.

The load and rms voltage vs. specimen deflection curves for an SL orientation sample of T-3 plate are shown in Fig. 7. The rms voltage curve contained numerous high amplitude spikes, commencing at the precrack load. Burst AE activities continued to be active until the maximum load was reached. The rms voltage level became lower beyond that point except for a few large spikes. The amplitude distribution data taken during the slow bend test of another SL sample of T-3 plate are shown in Fig. 8. Again, cumulative distribution is plotted against the peak amplitude of AE signals. The observed data above 20 μV can be fitted to a Weibull-type function[1,17,24,26]

Table 2. Energy Absorbed, E_a (J)

	T-1	T-2	T-3	T-4	T-5
LT	167.5	167.1	144.7	240.6	231.8
LS	178.9	172.6	271.8	243.7	256.2
TL	83.3	95.4	52.5	112.6	108.5
TS	92.7	99.2	68.7	114.6	118.8
SL	59.8	--	24.9	69.2	61.0
ST	67.9	86.7	26.8	58.8	61.0

Table 3. Cumulative AE Event Counts up to 2.54mm in Specimen Deflection

	T-1	T-2	T-3	T-4	T-5
LT	140	52	560	120	134
LS	132	230	3320	656	700
TL	136	57	1360	132	144
TS	168	650	4830	870	890
SL	110	960	11800	3490	3220
ST	130	1240	11700	3080	4080

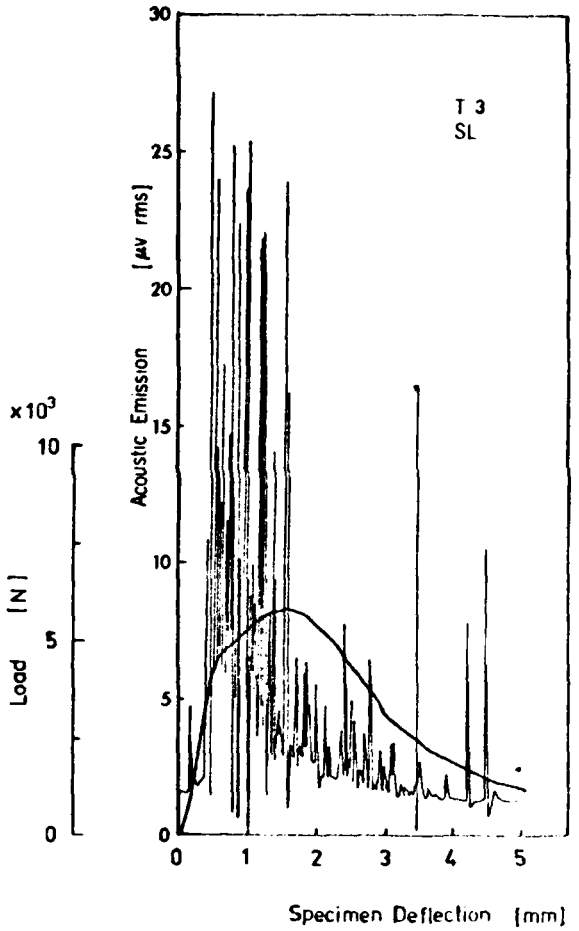

Fig. 7 Stress and AE level against specimen deflection for Charpy slow bend test in SL specimen of T-3 steel.

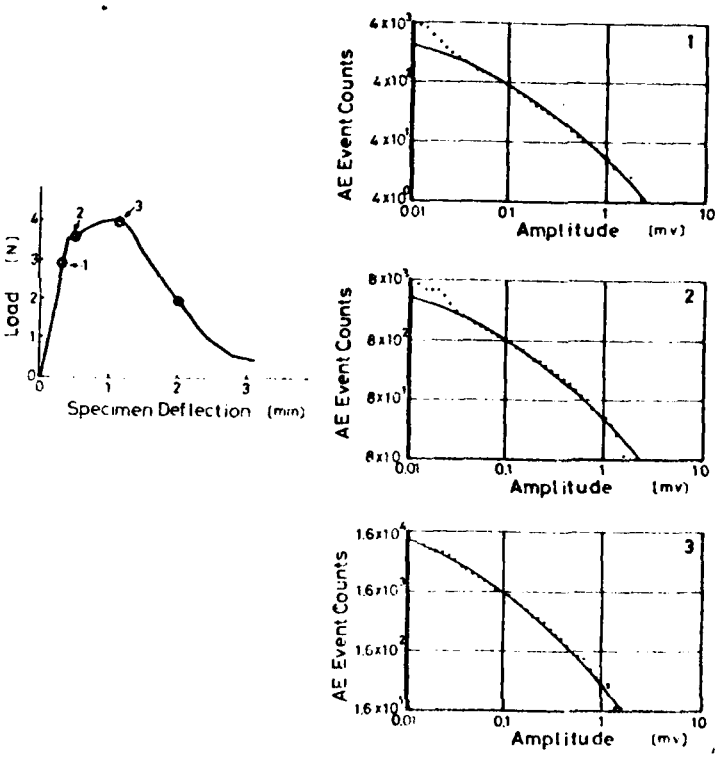

Fig. 8 Cumulative AE event during Charpy slow bend test in SL specimen of T-3 steel. Load-deflection curve also shown.

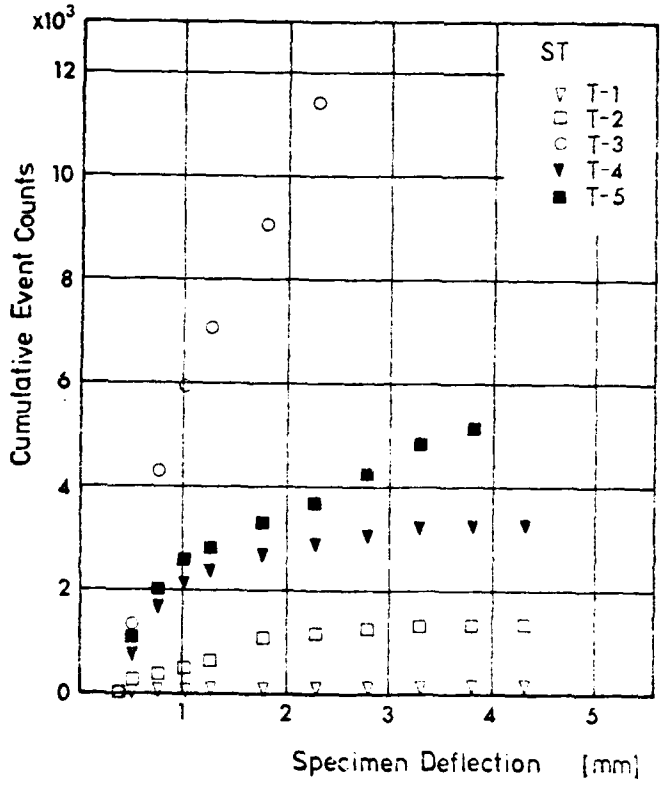

Fig. 9 Cumulative AE event counts against specimen delfection for Charpy slow bend tests in the ST orientation of five different plates.

$$F_3(V_p) = C \exp(-C' V_p^q), \qquad (3)$$

where F_3 is the amplitude distribution, C and C' are scaling constants and q is the shape factor. Curve drawn in Data 1 corresponds to Eq. (3) with q = 0.5 and those in Data 2 and 3 with q = 0.35. The deviations seen at low amplitudes in Data 1 and 2 appear to arise from the continuous AE present near the general yield load.

The AE behavior of low sulfur plates T-4 and T-5 was quite similar to that of T-3 plate except for lower N_e values. From the rms voltage-deflection curves, it is difficult to distinguish these samples. As Fig. 8 and Table 3 indicate, however, AE event counts clearly were reduced by 2 to 4 times in the ST and SL orientations. The reductions was even greater in other orientations. In Fig. 9, AE event counts for the ST orientation samples of high sulfur (open symbols) and low sulfur (filled symbols) plates are plotted against specimen deflection. T-3, T-4 and T-5 plates can be compared directly, as these received essentially identical rolling reduction. It is evident that AE event counts are proportional to the sulfur content, as N_e for T-3 is about three times that for T-4 or T-5. Difference between T-4 and T-5 is the finish roll temperature. Apparently, the present AE tests revealed no significant change between the two plates.

3. Interpretation and Discussion

Since burst emissions were most profusely emitted in the pre-yield region in the S direction tensile samples (cf. Ref. 15,17), it is not surprising to find AE activities near the general yield region. With an increase of sample deflection, a larger volume of the sample ahead of the plastic zones reaches the stress level that results in AE generation. AE activities continued beyond the maximum load in slow bend Charpy tests, where macroscopic crack growth is expected. This behavior is in sharp contrast to that found in the post-necking region in all the tensile tests where almost no AE was observed. These opposite trends imply that void coalescence produces no AE and that AE activities in slow bend Charpy tests originate from the nonmetallic inclusions both before and after the maximum load is reached. Observation on amplitude distribution analysis also supports this contention, and refutes the contribution due to crack extension to observed AE.

Effects of the sulfur content existed in all the six orientations of comparably rolled plates of T-3 and T-4. This indicates that manganese sulfide inclusions are always responsible for the observed emission in the slow bend Charpy tests. The ratio of the sulfur contents was 3 to 1, which suggests that the numbers of AE generating inclusions also have a similar ratio, when the size distributions are comparable. Thus, the observed ratio of about 3 of AE event counts in two materials in the SL and ST orientations can be considered to reflect the relative numbers of manganese sulfide inclusions. Even larger ratios (4 to 10) were observed in other orientations.

The decohesion of an inclusion is caused by the normal stress acting on the broad face of the inclusion. In bending, the main components of stress ahead of the crack tip are σ_y and to a lesser extent σ_x. In Group A orientations, σ_y acts normal to the broad faces of flattened manganese sulfide inclusions, whereas σ_x acts normal to the inclusion faces in Group B orientations. Thus, we expect higher AE activities in Group A than in Group B, which agrees with experimental findings. In Group C orientations, the only normal component that acts on the inclusion faces is σ_z, which is expected to be small in relatively thin samples, such as Charpy specimens. Thus, AE activitiy rating is the lowest for Group C. Considering the relative magnitudies of σ_y, σ_x and σ_z, we conclude

that the observed anisotropy originates from the changes in debonding tendency produced by crack tip stresses on extant nonmetallic inclusions, in particular flattened manganese sulfide inclusions.

In the above consideration, we attributed the observed AE characteristics to the inclusion debonding model. As noted earlier, amplitude distribution provides an additional support for the model. Since the Weibull distribution describes burst-type AE signals in both tensile (S direction [17]) and most of slow bend Charpy tests and it is identical to that derived from AE theory and the size distribution of manganese sulfide inclusions,[24] we can consider the sources of AE to be always the debonding of these inclusions. This is also consistent with fracture surface observations.

In the case of the power-law distributions observed in ADA of Groups B and C, in the low sulfur material the extreme value functions may be introduced to correlate the distribution laws to the statistical nature of microstructural parameters.[13] However, no acceptable prediction of the exponents can be made at present.

Finally, certain trends exist between absorbed energy and AE event counts at the maximum load. In general, high N_e is associated with low E_a and vice versa. However, large discrepancies of E_a in Groups B and C orientations are also evident. That is, LS orientation has a similar N_e as TS, but has a higher E_a than TS. This effect appears to be due to more favorable crack blunting effects of the inclusion in LS, whereas the width of the inclusions in TS is probably not wide enough to contribute to crack blunting. A similar trend exists between LT and TL, although less active in terms of AE.

IV. CONCLUSIONS

(1) AE behavior of SM50 steels indicates three distinct types of processes producing AE signals. These are the plastic deformation of the ferrite matrix, giving rise to continuous emissions mainly during yielding, the debonding of flattened manganese sulfide inclusions, emitting burst-type signals with the peak amplitude distribution of a Weibull character, and the second type of burst emissions whose origin is unclear.

(2) Burst-type AE during the ductile fracture of SM50 steel is primarily from the debonding of manganese sulfide inclusions. Sulfur content and orientation dependencies of AE and mechanical properties provide the major support for this conclusion.

(3) It appears reasonable to suggest that burst emissions observed in most fracture/AE testing of ductile structural steels also originate from the debonding of nonmetallic inclusions.

ACKNOWLEDGEMENT

The authors are grateful for the support of this work by the Physics Program, the Office of Naval Research, by the Sumitomo Heavy Industries, Ltd., Hiratsuka, Japan through the fellowship to one of them (M.Y.), by Nippon Kokan K.K. Kawasaki, Japan. They also acknowledge the technical and financial contributions of Acoustic Emission Technology Corp. Sacramento, California. Experimental assistance of Messers. R. Landy, S.S.Y. Hsu and H.B. Teoh is appreciated.

REFERENCES

1. K. Ono and M. Yamamoto, Mat. Sci. and Engr. (in press).

2. T.F. Drouillard, "Acoustic Emission, a Bibligraphy with Abstracts," Plenum Press, New York, (1979).

3. H.L. Dunegan, D.O. Harris and C.A. Tatro, Engr. Fracture Mech., 1, (1968) 105-122.

4. I.G. Palmer and P.T. Heald, Mat. Sci. Engr., 11, (1973) 181-184.

5. L.J. Graham and G.A. Alers, Mat. Eval., 32, (1974) 31-37.

6. Y. Nakamura, C.L. Veach and B.O. McCauley, "Acoustic Emission," ASTM STP-505, ASTM, Philadelphia, 1971 pp.164-186.

7. A.S. Tetelman, UCLA-ENG-7249, (1972), pp.1-44; also "Proc. US - Japan Joint Symp. on AE," High Press. Inst., Tokyo, (1972), pp.1-44.

8. C.E. Hartbower, W.W. Gerberich, W.G. Reuter and P.P. Crimmins, Engr. Fracture Mech., 1, (1968) 291-308.

9. J.D. Desai and W.W. Gerberich, Engr. Fracture Mech., 7, (1975) 153-165.

10. H. Nakasa, "Nucl. Power Plant Control and Instrumentation 1973," IAEA Publ. STI/PUB/34-1, IAE, Vienna, 1973, pp. 461-478.

11. M. Mirabile, "Proc. Conf. Fracture Mech. Tech.," Hong Kong, March 1977.

12. G. Clark and J.F. Knott, Met. Sci., 11, (1977) 531-536.

13. H.L. Dunegan and A.S. Tetelman, Engr. Fracture Mech., 2, (1971) 387-402.

14. R.R. Corle and J.A. Schliessmann, Mat. Eval., 31, (1973) 115.

15. K. Ono, H. Hatano and G. Huang, "Proc. 8th World Conf. NDT," Sec. 3K, Paper 3K3, Cannes, France, Sept. 1976, pp.1-10.

16. K. Ono, G. Huang and A. Kawamoto, "Internal Friction and Ultrasonic Attenuation in Solids," Univ.Tokyo Press, Tokyo, 1977, pp. 829-834.

17. K. Ono, R. Landy and C. Ouchi, "Proc. Fourth AE Symp.," Int. Tech. Exc. Center, Tokyo, 1978, pp. 4-33 - 4-45.

18. J. Holt and D.J. Goddard, CERL Notes RD/L/N82/79, 1979.

19. J. Holt and D.J. Goddard, "Proc. AE Symp." D.G.f.M., Bad Nauhein, Frankfurt, 1979.

20. D.V. Wilson, Metals Tech., 2 (1975) 8-20.

21. I. Kozasu and J. Tanaka, "Sulfide Inclusions in Steel," edited by J.J. de Barbadillo and E. Snape, Amer. Soc. Metals, Metals Park, Ohio, 1975, pp. 286-308.

22. T.J. Baker, "Sulfide Inclusions in Steel," edited by J.J. de Barbadillo and E. Snape, Amer. Soc. Metals, Metals Park, Ohio, 1975, pp. 135-138.

23. W. Dahl, Stahl u. Eisen, 97, (1977) 402-409.

24. K. Ono, "Fundamentals of AE," Univ. Calif., Los Angeles, 1979, pp. 167-207.

25. H. Nakasa, "Proc. 4th AE Symp.", Int. Tech. Exc. Center, Tokyo, 1978, pp.4-1 - 4-21.

26. R. Landy, ONR Tech. Rep. 79-02, Univ. Calif., Los Angeles, 2979, pp. 1-103.

27. Y. Hirai, J. Tsuboi and K. Kobayashi, "Proc. 3rd Int. Symp. JWS," Japan Joint Symp. on AE," High Press. Inst., Tokyo, 1972, pp. 1-44.

TEMPERATURE DEPENDENCE OF ANISOTROPIC AE BEHAVIOR OF A533B STEEL

K. Okajima and K. Ono
Department of Materials Science and Engineering
School of Engineering and Applied Science, U.C.L.A.
Los Angeles, California 90024

ABSTRACT

It has been established that acoustic emission (AE) behavior during mechanical testing of hot-rolled steels is sensitive to the number, size and distribution of nonmetallic (mainly MnS) inclusions. Effects of the inclusions are particularly conspicuous in the thickness (short transverse) direction. In this study, AE measurements were performed during tensile tests of ASTM A533B steel in order to investigate the influence of test temperature and thermal stress at the interface between matrix and MnS inclusions on the anisotropy of AE characteristics. Several different AE parameters, i.e., rms voltages, event counts, event count rates, and amplitude distributions were employed. Test temperature was from -150°C to 150°C.

Burst type AE signals observed in the test of thickness direction samples have been attributed to the decohesion of the elongated MnS inclusions. When test temperature was varied, the identical burst type amplitude distribution of Weibull type and the rms peak voltage that was observed before the yield point were quite similar. This lack of temperature dependence is an expected consequence of the inclusion debonding in the steel. On the other hand, AE signals in the test of longitudinal direction samples consisted mostly of the continuous type. These were weaker than the burst emissions and several different types of amplitude distributions were exhibited as test temperature was changed. The peak rms voltages, usually appeared at the yield point, increased with test temperature. These effects originate from plastic deformation or the motion of dislocations. As the speed of screw dislocations is lower, AE is weak at lower temperatures in bcc metals. With increasing test temperatures, faster dislocations become abundant with higher AE levels expected.

Thermal stresses at the inclusion interfaces were varied by changing the cooling rate of the final stage of the heat treatment without altering the microstructure. The stresses σ_p, at which rms voltage reached a maximum, was influenced by the thermal stresses and decreased with increasing thermal stress. Assuming the existence of the critical stress for decohesion, the present results can be explained on the basis of elasticity theory and calculations of Eshelby and Shibata and Ono.

I. INTRODUCTION

Previous studies have established that acoustic emission (AE) behavior during the mechanical testing of low alloy steels is sensitive to the number, size and distribution of nonmetallic inclusions.[1-5] Effects of the inclusions are particularly conspicuous in the thickness or short transverse direction. Burst type AE signals observed in the test of the thickness direction samples have been attributed to the decohesion of the elongated MnS inclusions. Amplitude distribution of the burst-type emissions from samples can be

esented by a Weibull type distribution function,

$$F_1 (V_p) = A \exp (-A' V_p^q) \qquad (1)$$

e F_1 is the cumulative distribution function, V_p is the peak amplitude of a t signal, A and A′ are scaling constants and q is the shape factor, ectively. The values of q were found to be 0.3 to 0.4 during the tensile fracture testing of A533B and SM50 steels. This distribution function was ific ally correlated to the size distribution of MnS inclusions via a theory E signal generation.[3,5]

Continuous-type AE signals were also observed in steel samples during oscopic yielding. These originate from the plastic deformation or the on of glide dislocations. In the thickness direction samples, continuous als contribute only a small fraction of observed AE activities. However, e constitute the major portion of AE activities in the longitudinally ssed samples. Amplitude distribution observed in the longitudinal direction les is represented by two distribution functions. One is the Weibull ribution function with the exponent, q = 4;

$$F_2 (V_p) = B \exp (-B' V_p^4) \qquad (2)$$

e B and B′ are constants. This represents the cumulative amplitude ribution of continuous random signals. Some burst activities were also rved. Their characteristic amplitude distribution obeys the power-law ribution function,

$$F_3 (V_p) = CV_p^{-n} \qquad (3)$$

e C and n are constants. The values of n were typically near unity. These t emissions are believed to come from nonmetallic inclusions.

The anisotropy of AE behavior in low alloy steels can thus be identified ugh the amplitude distribution analysis and traced to the distribution of etallic inclusions. In this study, we wish to extend our understanding on anisotropic AE behavior of A533B steel under uniaxial tension. Two new ables are introduced; test temperature and the state of thermal stresses at interfaces of the nonmetallic inclusions and matrix. Temperature and stress ndencies of various AE characteristics have been clarified and are to be ussed in this paper.

II. EXPERIMENTAL PROCEDURES

ASTM A533B class 1 steel, which has the chemical composition of 0.18 C, Si, 1.43 Mn, 0.013 P, 0.005 S, 0.50 Mo, 0.66 Ni, 0.28 Cr and 0.01 Cu, was in this study. The starting stock was 165 mm thick plate, supplied by on Steel Corp.

Half size ASTM standard E8-69 tensile specimen (6.35 mm gauge diameter, 32 educed section length and 90 mm overall length) were used in this study. specimens were machined with axial direction parallel to the longitudinal and to the thickness (Z) direction of the steel plate. After machining, the lmens were austenized at 930°C for one hour in a vertical three-zone stance wound furnace in vacuum, and were cooled to room temperature in m within 30 minutes. The specimens were then tempered in the same furnace 50°C for 24 hours. Three different cooling rates, namely furnace cool (FC), cool (AC), and water quench (WQ) were used for the final cooling stage from C to room temperature, in order to change the magnitude of the thermal sses on the MnS inclusion-matrix interfaces.

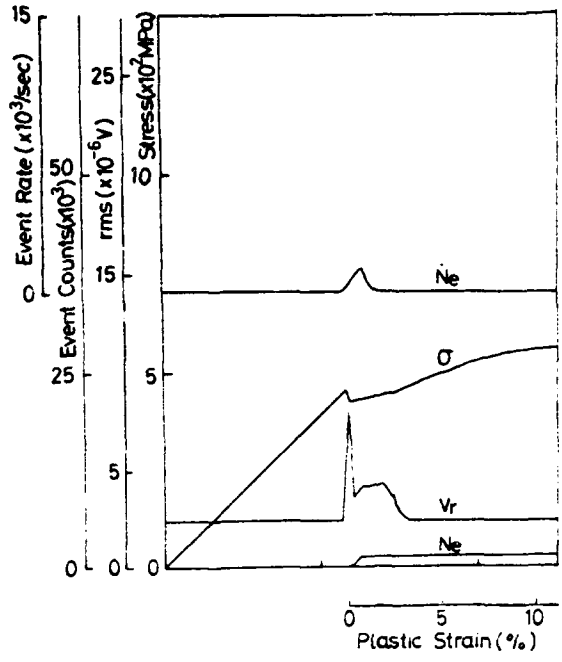

Fig.1 AE activities of L-AC sample at 25°C.

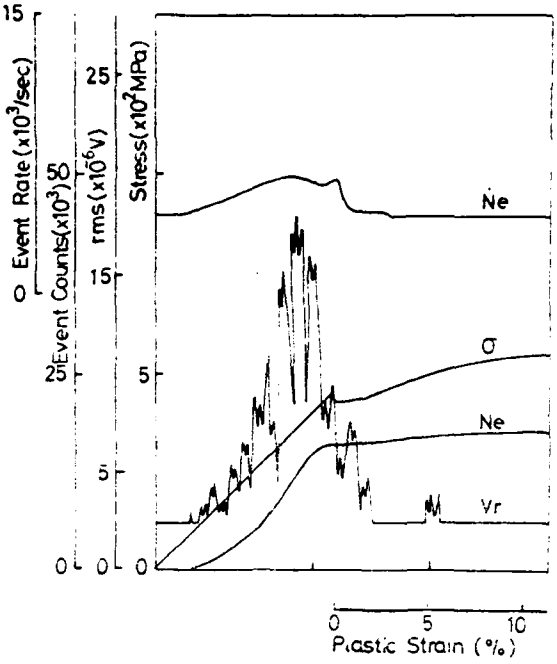

Fig.2 AE activities of Z-AC sample at 25°C.

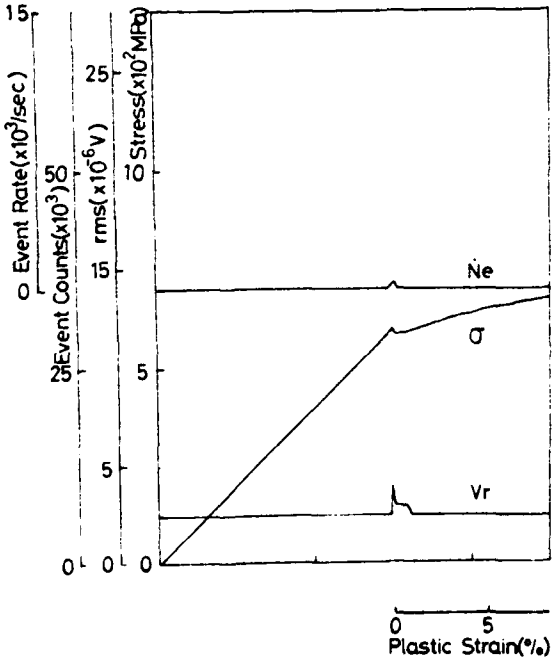

Fig.3 AE activities of L-AC sample at -150°C.

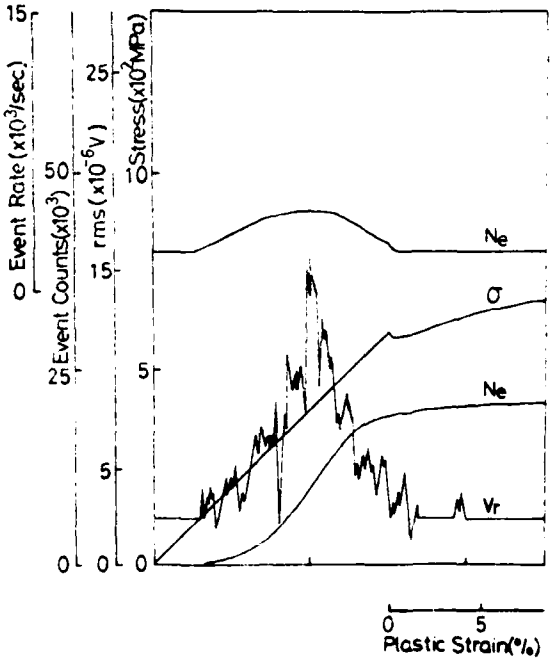

Fig.4 AE activities of Z-AC sample at -150°C.

All tensile tests were performed using a floor model Instron. Tests were conducted over the temperature range -150°C to 150°C and with crosshead speed of 0.021 mm/sec or the nominal strain rate of 0.7×10^{-4} sec^{-1}.

The AE transducer used in this experiment was resonant-type with a nominal center frequency of 175 KHz (AC 175L, AET). A bandpass filter of 125 -250 KHz was used in the preamplifier (160, AET). The input noise level was 2.2 μV. On-line amplitude distribution analysis of AE signals was performed using amplitude distribution analyser (203, AET), which provided the cumulative event counts and the amplitude distribution. The latter was displayed on an oscilloscope and recorded photographically.

III. RESULTS

Figures 1 to 6 show AE activities during the tensile tests. Here, the rms voltages (V_r), AE event counts (N_e) event rates ($\dot{N}_e$) and applied stress are plotted against time, which is equivalent to the crosshead displacement of the Instron.

Observed AE behavior of L-AC samples (the longitudinal direction; air-cooled after 650°C tempering) at 25°C was similar to the well-known AE characteristics of a mild steel; i.e., AE activities were significant only during Luders deformation or the initial yielding and became very low or zero after work hardening began. This is shown in Fig. 1.

AE activities in the Z direction samples showed totally different behavior from those in the L direction samples. Figure 2 presents the AE behavior of a Z-AC sample at 25°C. AE signals rose above the background at about 100 MPa. Both N_e and V_r increased to much higher levels than those in the L-AC sample (Fig. 1). The V_r-time curve consisted of numerous spikes. $\dot{N}_e$ exhibited two peaks. The first peak appeared at about 400 MPa, where the envelope of the Vr-time curve also had a peak. The second peak of $\dot{N}_e$ coincided with the yield point. The shape and level of this peak was similar to those of the peak which was observed in the L-AC sample. Although the V_r-time curve did not exhibit the second peak, the sharp spike which appeared at the yield point had the same magnitude as that observed in the L-AC sample. AE activities persisted at lower levels during work hardening, in contrast to no AE activities in the L-AC samples. Event counts reached 20,000, 70% of which was produced during the elastic loading. Note that no AE was observed in the L direction samples before the yield point.

AE activities of an L-AC sample at -150°C is shown in Fig. 3. The stress vs. time curve was similar to that at 25°C except for a higher yield strength. The AE activities were quite low even during the yield drop and Luders deformation. Event counts were too low to appear in this figure.

Figure 4 shows AE behavior of a Z-AC sample at -150°C. AE activities were high during the elastic range. AE signals started to appear at about 100 MPa. $\dot{N}_e$ and V_r each had a maximum at about 400 MPa. These two stress levels were the same as those in the Z-AC sample at 25°C. At -150°C, the second peak of $\dot{N}_e$ was not observed at all. The peak value of $\dot{N}_e$ was about 2000 sec^{-1}, which was identical to that in the Z-AC sample at 25°C. Event counts reached 22,000, which was 10% larger than that at 25°C. 90% of N_e were generated during the eleastic loading.

The AE activities in an L-AC sample were quite high at 150°C as shown in Fig. 5. V_r and $\dot{N}_e$ reached a maximum at the yield point. Although AE beyond yielding was very active at this temperature, no AE signal was observed until the yield point.

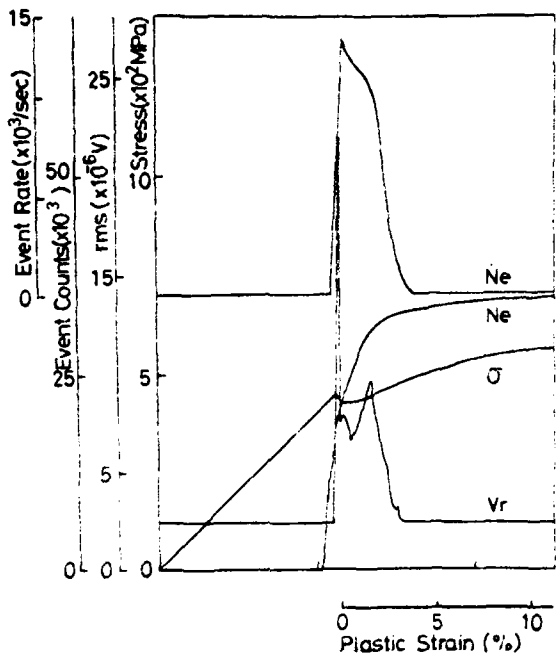

Fig.5 AE activities of L-AC sample at 150°C.

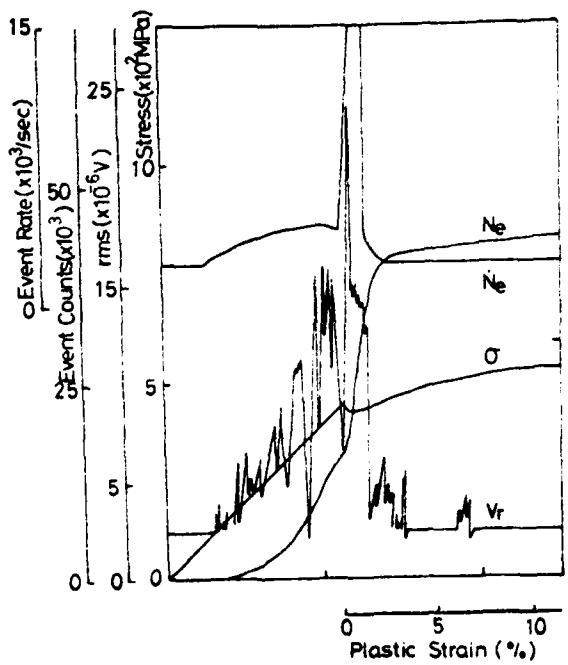

Fig.6 AE activities of Z-AC sample at 150°C.

AE behavior of a Z-AC sample at 150°C is shown in Fig. 6. Again, AE signals began to appear at about 100 MPa, and $\dot{N}_e$ and V_r had the first peak at about 400 MPa. Not only $\dot{N}_e$ but also V_r had the second peak, coinciding with the Luders deformation. The peak levels were consistent with those of an L-AC sample at 150°C. Event count was 45,000, 40% of which were generated before the yield point.

Waveforms of AE signals during tensile tests were observed in situ on an oscilloscope. AE signals generated in the L direction samples consisted mainly of continuous-type emission. On the other hand, most of the observed AE signals in the Z direction samples consisted of burst-type emission, especially below room temperature.

In order to investigate the AE signals quantitatively, amplitude distribution analyses were conducted during each AE test. The results of amplitude distribution analyses for the L-AC samples at -150°C, 25°C, and 150°C are shown in Fig. 7 a, b, and c respectively. Here, cumulative AE event counts are plotted against the peak amplitude (equivalent preamplifier input voltage). Each amplitude distribution analysis was obtained during Luders deformation. Since the threshold level was chosen to be 20 μV, low amplitude part exhibited a horizontal line. This precluded the appearance of weak continuous components in tests below 25°C. For tests at 150°C, the cumulative amplitude distribution for continuous emission, $F_2(V_p)$, was observed (see Fig. 7c and Eq. (2)). The amplitude distribution in Fig. 7 a and b can be expressed by a power law of Eq. (3) with n = 1.0.

In the Z direction samples, the amplitude distribution analyses of AE signals produced entirely different results, as shown in Fig. 8. The observed amplitude distribution functions at -150°C, 25°C, and 150°C can be represented by Eq. (1) with q = 0.3.

Since AE signals in the L direction samples were mainly continuous, $\dot{N}_e$ and N_e are not suitable AE parameters. Peak values of V_r at yielding fluctuated from sample to sample. Therefore, the overall level of AE activities can best be described by ΣV_r, which is the integration of V_r above background. In Fig. 9, ΣV_r is shown as a function of test temperature. In the Z direction sample, most AE signals consisted of burst type emission. Here, $\dot{N}_e$ and N_e are the suitable AE parameters to measure the intensity of AE activities. Figure 9 also shows $\dot{N}_e$ of the first peak for the Z direction samples as functions of test temperature. It is seen that ΣV_r increases with test temperature and that cooling rate has no effect on ΣV_r. On the other hand, the maximum event rate exhibited no significant temperature dependence. However, no effect of heat treatment was observed for the maximum event rates.

While totalized event counts, ΣN_e, can provide a good measure of burst-type signals, it also includes the contributions from continuous emission. Reflecting higher AE activities due to yielding with increasing test temperature, ΣN_e increased dramatically above 25°C, especially in the L direction samples (see Fig. 10). While it included small contributions of burst emissions with the power-law amplitude distribution, the totalized event counts for the L direction samples, $\Sigma N_e(L)$, can be employed to deduce the true counts of burst emission, N_{eb}, by

$$N_{eb} = \Sigma N_e(Z) - \Sigma N_e(L) \qquad (4)$$

This procedure can be justified by noting the similarity in $\dot{N}_e$ during yielding between the L and Z direction samples; i.e., the continuous contributions are independent of orientation. Figure 10 shows N_{eb} thus obtained as functions of test temperature. N_{eb} decreased about 10% with increasing temperature from -150 to 150°C. Effects of heat treatment appeared as parallel shifts of the N_{eb} vs

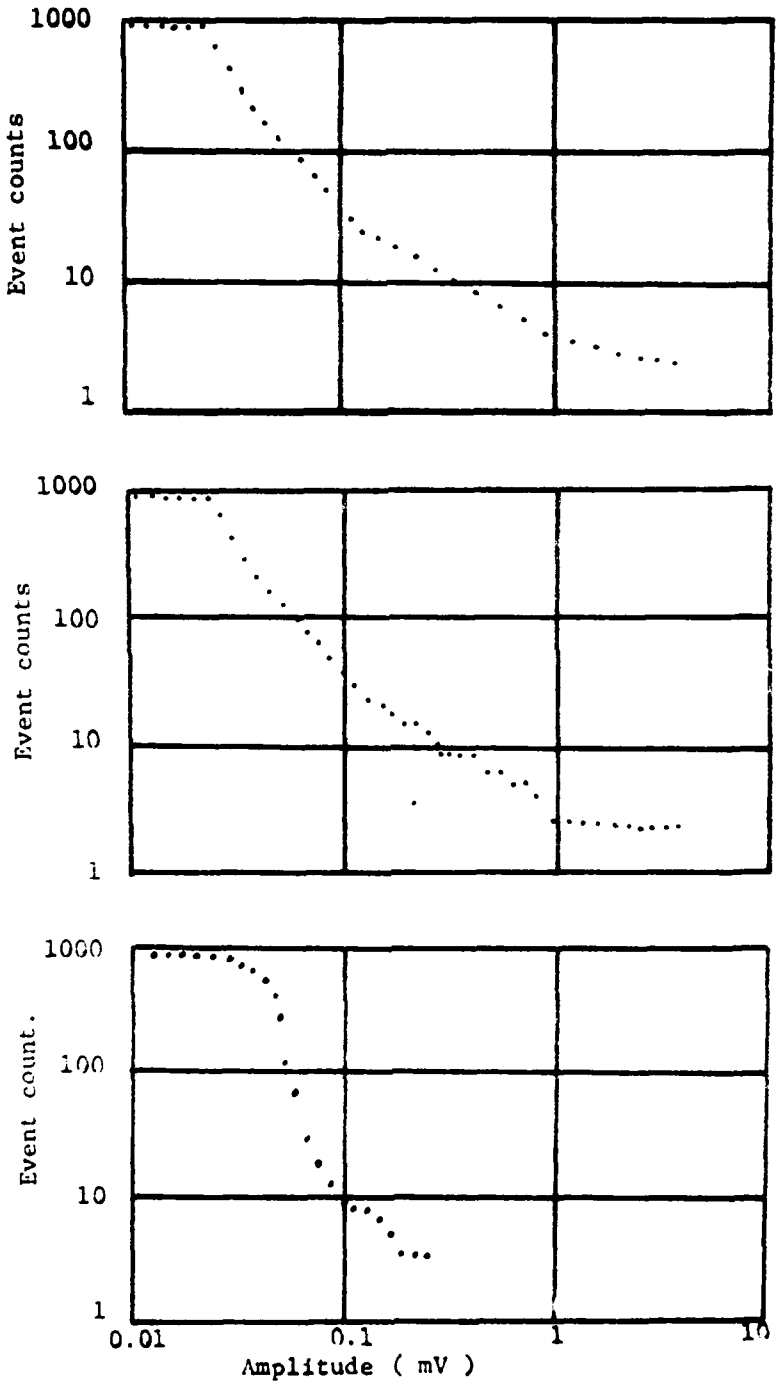

Fig.7 Amplitude distribution of L-AC samples at a.-150°C, b.25°C, c.150°C, respectively.

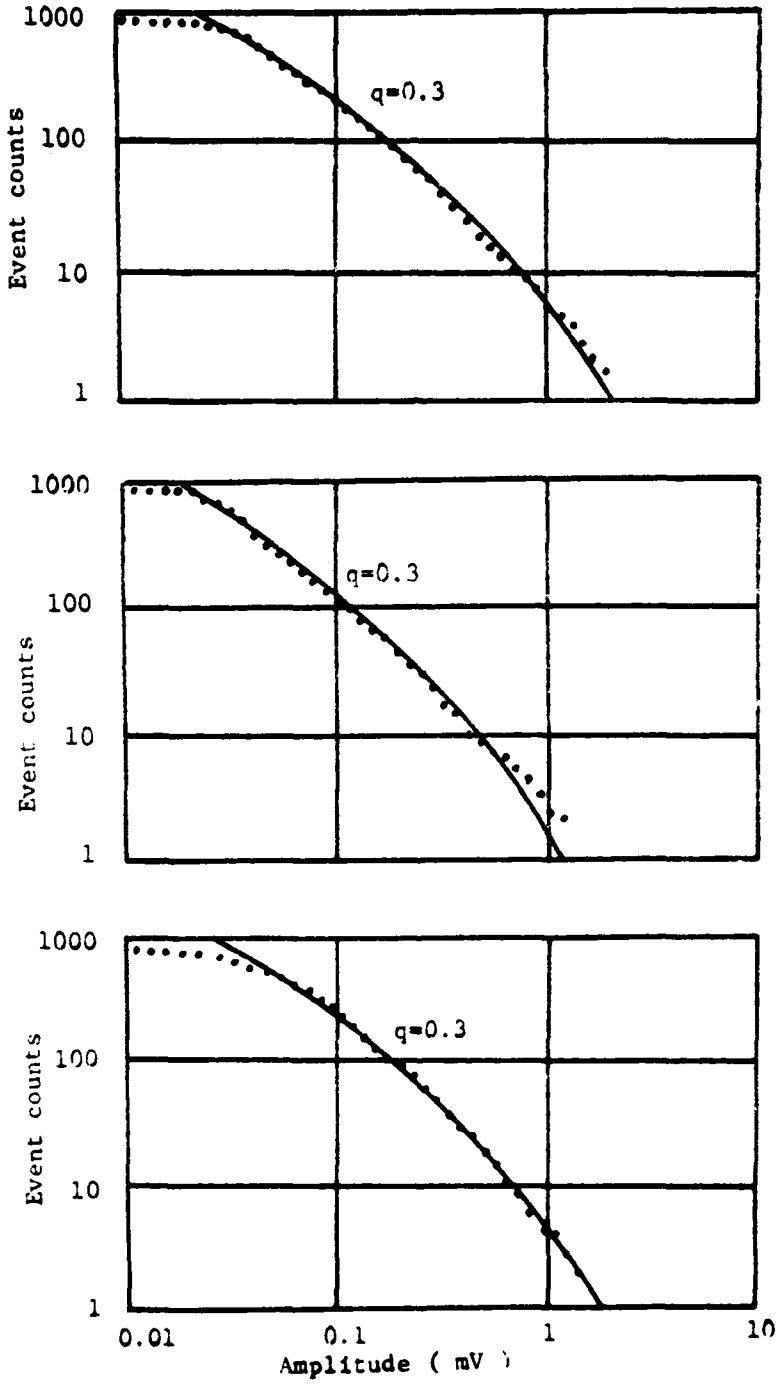

Fig.8 Amplitude distribution of Z-AC samples at a.-150°C, b.25°C, and c.150°C, respectively.

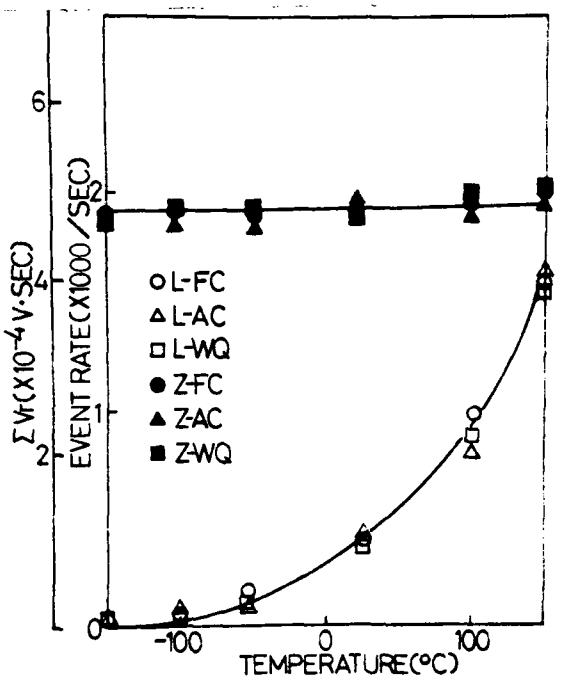

Fig.9 Integrated rms voltage, ΣVr, of the L direction samples and the peak value of the event rate, Ṅe, of the Z direction samples as functions of test temperature.

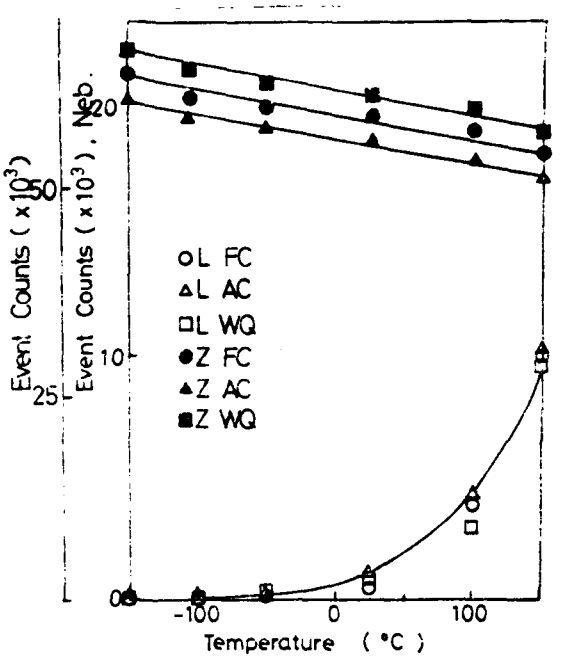

Fig.10 Event counts, Neb, due to burst emissions of the Z direction samples, and event counts, Ne, of the L direction samples as function of test temperature.

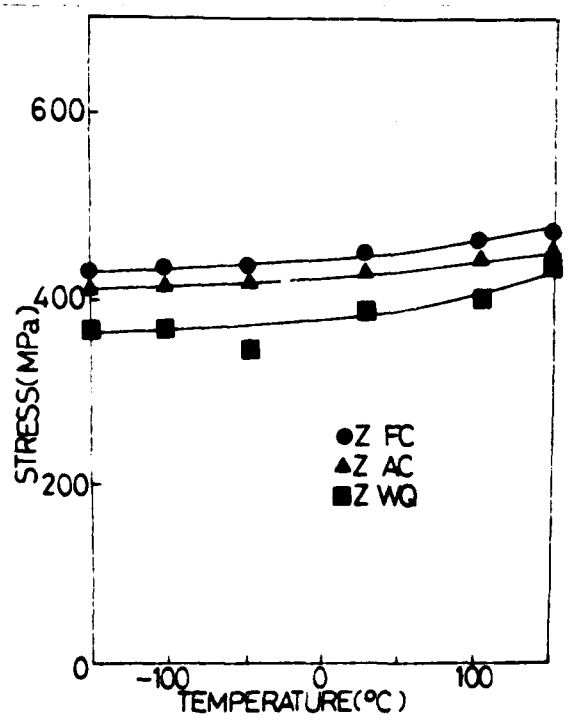

Fig.11 Stress, σp, at which Ṅe has the first peak as functions of test temperature.

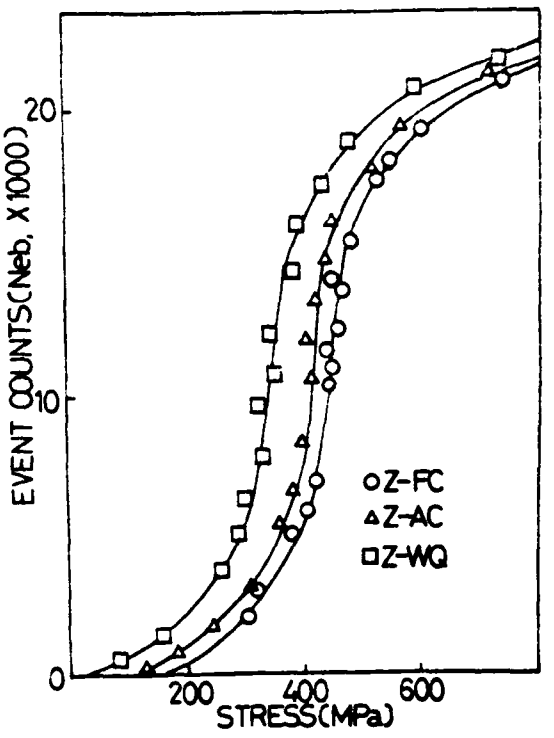

Fig.12 Event counts, Neb, due to burst emission as function of applied stress.

temperature curves. Z-FC samples were the lowest and Z-WQ samples were the highest. The difference was at most 10%, however.

Stress, σ_p, at which the first peak of $\dot{N}_e$ appeared in the Z direction samples, increased slightly with test temperature (see Fig. 11). Heat treatment affected the σ_p vs temperature curves, shifting that of Z-FC samples to the highest and that of Z-WQ samples to the lowest.

In summary, the results of AE and tensile testing indicate:

1) ΣV_r and ΣN_e of the L direction samples increased with test temperature, but they were unaffected by the post-tempering cooling rate.

2) N_{eb} of the Z direction samples decreased with slower cooling after tempering and was nearly independent of test temperature.

3) The first peak of $\dot{N}_e$ of the Z direction samples had a constant height regardless of test temperature and cooling rate.

4) σ_p of the Z direction samples increased with higher test temperature and with lower cooling rate.

5) Amplitude distribution of AE in the L direction samples was independent on cooling rate, but varied with test temperature from the power-law to that of continuous emission.

6) Amplitude distribution of AE in the Z direction samples was independent of test temperature and cooling rate, showing the characteristic Weibull function (Eq. 1).

IV. DISCUSSION

Large temperature effects on the AE activities at the yielding were observed in this study. The observed activities were unaffected by the orientation. This is expected since plastic deformation if the source of the emissions. For the same reason, the lack of heat treatment effect is understandable because of the absence of microstructural changes. Because of strong burst emission activities in the Z direction samples, the effects were not as clearly shown as in the L direction samples. The trend of higher AE activities with increasing temperature agrees with other studies.[6-9] In comparison to Hsu's work on iron,[7] however, the extent of the observed increase was much higher. Nearly vanishing AE activities at -150°C were also surprising, although no comparable data exists. Results of amplitude distribution analysis reflected the variation of continuous emission activities. At low temperatures, the continuous contribution was hidden by the threshold level selected, but it emerged unmistakabley at 150°C.

While exact causes of the observed temperature dependence are not readily deduced, we may suggest a few probable origins. In basically ferritic microstructures as A533B steel, we expect the motion of screw dislocations to be the rate-controlling step for plastic flow below room temperature. This has been recognized as the source of strong temperature dependence of the yield strength in bcc metals. The dislocation motion in bcc metals at low temperature is typically modelled by thermally activated nucleation and growth of a double-kink. Consequently, it is unlikely for dislocations to move at high speeds and the magnitude of instantaneous plastic strain increment cannot be large. According to a recent theory of continuous AE, this leads to low AE levels.[8]

Above room temperature, the dislocation substructures after deformation are similar in bcc and fcc metals, indicating diminished effects of screw dislocation as the sole rate-controlling step. Yet the AE levels at yielding above 50°C increased rapidly. This effect cannot be attributed to the behavior of screw dislocations. More gradual increases of AE levels with temperature can be ascribed to the changes in internal stress fields according to Hsu.[7] Again, the observed increases in A533B steel were too large to rationalize on this basis. Since dislocation in tempered A533B steels are expected to have strong Cottrell atmospheres and the unpinning of the existing dislocation sources must preceed plastic flow, it is possible that the unpinning at higher temperatures occurs at fewer strongly pinned sources. It follows then that the number of activated sources becomes smaller, as the plastic strain increments are larger while the strain rate remains constant during a tensile test. According to Ono,[8] this leads to higher levels of continuous AE.

Burst emission activities were relatively unaffected by test temperature. when the event counts due to continuous emssions were excluded, the number of burst emissions, N_{eb}, varied little with temperature. The amplitude distribution also remained unchanged and the majority of burst emissions was observed in the elastic loading range. These characteristics are anticipated consequences of the inclusions debonding model. Our present results again give credence to the validity of the model. Quantitatively, our results are in good agreement with previous investigatins[1-5] as to the number of burst emissions and the parameters of amplitude distribution functions.

Stress dependence of burst emission activities in the Z direction samples was most interesting. While effects of test temperature were minimal, the post-temper cooling rate produced notable and consistent effects on the stress dependence. When cumulative burst emission counts, ΣN_{eb}, was plotted against stress, the data fell on a single curve for each cooling rate regardless of test temperature; i.e., three curves were obtained for three heat treatment conditions (FC, AC and WQ, respectively). This is shown in Fig. 12. Note also that these can be shifted on the stres axis to yield a single master curve. Normalizing the cumulative counts by a maximum value, N_{max} the stress dependence can be approximated by

$$\Sigma N_{eb}/N_{max} = 1 - \exp(-(\sigma - \Delta\sigma)^4/\sigma_o^4), \qquad (4)$$

where σ_o is a scaling constant and $\Delta\sigma$ is the stress shift. The maximum shift was 80 MPa.

The existence of a single stress function implies that the decohesion is controlled by the stress at the inclusion-matrix interface, and is not dependent of plastic deformation of the matrix. Since most burst emissions were found below the yield stress, this conclusion is reasonable although the plastic deformation of the matrix can produce additional emission beyond yielding. When the internal stress is calculated assuming the thermal stress to be the major component,[10-12] we find the stress shift of 80 MPa corresponds to temperature differential of 270°C. That is, water-quenched samples possessed the tensile interface stress 110 MPa higher than that in furnace-cooled ones and the temperature at which the inclusion and matrix had been in equilibrium before cooling was 270°C higher in the WQ samples than in the FC samples. This calculated temperature difference appears to be consistent with the relative severity of the cooling treatments.

V. CONCLUSIONS

1. Large effects of test temperature were found in continuous AE activities due to plastic yielding of normalized and tempered A533B steel samples

irrespective of their orientation.

2. Burst emission activities in the thickness direction samples were unaffected by test temperature, but the cooling rate following tempering varied the stress level of the maximum burst emission rate.

3. Cumulative burst emission counts can be described by a single function of stress when the thermally induced internal stress at the inclusion-matrix interface is accounted for.

ACKNOWLEDGEMENTS

This research was supported by the ONR Physics Program and by Acoustic Emission Technology Corp., Sacramento, California. One of the authors (K. Okajima) acknowledges the financial assistance by the Graduate Student Fellowship of the Ministry of Education of Japan. Steel plate used in this study was dontated by Nippon Steel Corp.

REFERENCES

1. K. Ono, H. Hatano and G. Huang, "Proc. 8th World Conf. NDT," Sec. 3K, Paper 3K3, Cannes, France, Sept. 1976, pp. 1-10.

2. K. Ono, G. Huang and A Kawamoto, "Internal Friction and Ultrasonic Attenuation in Solids," Univ. Tokyo Press, Tokyo, 1977, pp. 829-834.

3. K. Ono, R. Landy and C. Ouchi, "Proc. Fourth AE Symp.," Int. Tech. Exc. Center, Tokyo, 1978, pp. 4-33 - 4-45.

4. K. Ono, M. Shibata and M.A. Hamstad, Met. Trans., 10A, (1979) 761-764.

5. K. Ono and M. Yamamoto, Mat. Sci. Engr. (in press).

6. G. Airoldi, "Proc. Inst. Acoustics Conf. on AE and Mat. Eval." April 1979, London.

7. S. Hsu and K. Ono, this Symposium.

8. K. Ono, "Fundamentals of Acoustic Emission," K. Ono, ed., Univ. Calif., Los Angeles, 1979, pp. 167-207.

9. T. Kishi and K. Kuribayashi, ibid., pp. 105-128.

10. J. D. Eshelby, Proc. Roy. Soc., A241, (1957) 376.

11. M. Shibata and K. Ono, Acta Met., 26, (1978) 921-32.

12. M. Shibata and K. Ono, Mat. Sci. Engr., 34, (1978) 131-37.


DATE:
ILME